August, 1983

PLASMA-VACUUM INTERFACE PROBLEMS IN MAGNETOHYDRODYNAMICS

J.P. Goedbloed

Plasma Fusion Center
Massachusetts Institute of Technology
Cambridge, Massachusetts 02139

PFC/JA-83-25

Plasma–Vacuum Interface Problems in Magnetohydrodynamics

J.P. Goedbloed*

Massachusetts Institute of Technology
Plasma Fusion Center, Cambridge, MA 02139

Abstract

A review of ideal MHD theory pertaining to thermonuclear confinement problems is presented, starting with fundamental questions concerning the spectrum and ending with optimization studies of high–β tokamaks.

---

*On leave of absence from FOM Institute for Plasma Physics, Nieuwegein, The Netherlands.

1. Introduction

In magnetic fusion research interface problems arise naturally from the requirement that a thermonuclear plasma be confined and isolated from the outside world by a vacuum magnetic field (Fig. 1). In the early investigations this goal was thought to be realizable by the technique of pinch implosion, leaving behind a hot plasma of high density and separated from the vacuum region by a sharp boundary layer in which skin–currents are flowing. Ideally, this interface represents a surface of discontinuity where the description of the state of the system changes abruptly. The plasma would be described as an infinitely conducting fluid, whereas the little material that is left behind in the outer region would be assigned zero conductivity.

Historically, this ideal picture has played an important role in identifying and analyzing the most global instabilities, like external kink modes, resulting in a violent destruction of the plasma as a whole. With the success of tokamak performance and the concomitant decline of θ–pinch research, the stress has shifted more to the analysis of diffuse plasma configurations where there is hardly any space left for regions that would qualify as a vacuum. As is always the case with changing fashions, this has tended to obscure some of the previous insights obtained from the sharp–boundary model and, also, it has led away from an area of research where there might have been more benefit from developments in other parts of fluid dynamics. [The latter insight dawned on the author while attending the International Conference on Fronts, Interfaces, and Patterns.]

This paper is an attempt at reviewing some of the developments in magnetohydrodynamics (MHD) as they are relevant to the subject of interfaces, both in a narrow sense as pertaining to the phenomena described by skin–current models and in a wider sense as pertaining to a description of the global plasma motion of confined, i.e., inhomogeneous plasmas. It should be added at this point that this review is strongly biased toward some aspects of spectral theory of 1D systems and methods of analyzing 2D problems where certain personal preferences are obvious [1]. Some of the older literature pertinent to the subject of ideal magnetohydrodynamic equilibrium and stability is found in Refs. [2,3]. For more up to date reviews of the subject matter the reader is referred to Refs. [4–6].

In Sec. 2 ideal MHD is introduced as a relevant model for the study of toroidal plasma confinement properties. Interface problems and characteristics are discussed in Sec. 3 to illustrate the complementarity of global and local approaches. Sec. 4 presents some of the basic issues of spectral theory of 1D MHD systems, in particular the gravitating slab and the diffuse linear pinch. In Sec. 5 some 2D toroidal confinement problems are outlined and a method of solving them by means of conformal mapping is discussed. Explicit results with respect to the stability of high–β tokamaks are presented in Sec. 6. Finally, some possibilities for future work are indicated in Sec. 7.

2. The Model of Ideal MHD

2.1. Experimental Starting Point: Toroidal Plasma Confinement

Our starting point is the task of properly describing the global properties of confinement of plasmas in toroidal geometry (Fig. 2), as considered for the purpose of CTR (controlled thermonuclear reactions).

First, let us introduce some of the usual terminology and parameters. Plasma confinement in tokamaks is effected by an externally created toroidal magnetic field B_φ, which is modified by the poloidal plasma current I_p, and a poloidal magnetic field B_p, which is created by the toroidal plasma current I_φ. The resulting configuration is characterized by helical magnetic field lines which are wound on toroidal magnetic surfaces nested around a single magnetic field line which is purely toroidal, the magnetic axis. For a toroidal tube of circular cross-section the geometry is fixed by the value of the inverse aspect ratio $\epsilon \equiv b/R$, which is extensively exploited as a small parameter in many theoretical investigations.

An important problem presented by this approach to plasma confinement is to find the spatial distribution of the magnetic fields, currents, energies, pressure, density, etc., and, in particular, to find the critical value of the parameter β,

$$\beta_{crit} \equiv 2\langle p\rangle_{max}/\langle B_\varphi^2\rangle_{min}, \tag{1}$$

in dependence of the safety factor

$$q \equiv \frac{1}{2\pi}\oint \frac{B_\varphi}{RB_p}dl \approx \frac{2\pi r^2 B_\varphi}{RI_\varphi}. \tag{2}$$

Here, $\langle p\rangle$ is the average plasma pressure and $\langle B_\varphi^2\rangle$ is the average squared toroidal field so that β present a figure of merit for a particular plasma confinement machine determining the amount of thermonuclear power output that is eventually to be expected.

The parameter q has a simple geometric interpretation (Fig. 3). It measures the average pitch of the magnetic field lines or the inverse rotational transform, which varies from one magnetic surface to the next. Hence, $q = q(\psi)$, where ψ is the poloidal flux which is a convenient radial coordinate to label the magnetic surfaces in toroidal geometry. In Fig. 3 we have depicted a particular magnetic surface on which $q < 1$ although usually $q > 1$ is required on all magnetic surfaces for stability of tokamaks.

An alternative interpretation of q is indicated in the approximate equality of Eq. (2), which is valid for $\beta \ll \epsilon \ll 1$ (so-called low-β tokamaks) and magnetic surfaces with circular cross-section. Here, the toroidal current I_φ appears in the denominator, so that low-q devices (e.g., reversed field pinches) correspond to large

toroidal current and high q corresponds to small toroidal current. For tokamaks $q \sim 1$. The important point to notice is that the expression on the right of Eq. (2) provides a more convenient parameter than q itself, when interpreted as a global parameter evaluated at the outermost magnetic surface, i.e., at the plasma–vacuum interface:

$$q^* \equiv \frac{2\pi a^2 B_\varphi}{R I_\varphi}. \tag{3}$$

Here, a is a measure for the radial dimension of the plasma column, usually taken to be the half-width in the equatorial plane. For so-called "high-β" tokamaks, where $\beta \sim \epsilon$, q^* may deviate appreciably from the value of q at the plasma surface.

We may now formulate one of the central questions of CTR: Find the distribution of the pressure p and of the magnetic field components B_p and B_φ, and of the associated current densities j_φ and j_p, such that the quantity β_{crit} defined in Eq. (1) is maximum. Concerning the parameter q^*, this optimization leads to conflicting requirements with respect to Ohmic heating and equilibrium of the plasma, where one would like to have q^* as small as possible (i.e., I_φ maximum) and stability of the plasma, where high q^* operation (i.e., I_φ minimum) is more desirable. A surprisingly large part of present day plasma theory is devoted to precisely this single question. Accordingly, the present paper will address a number of interesting theoretical issues, but always aiming at a contribution to the solution of this question.

2.2. Requirements for a Theoretical Model

In order to solve the mentioned problems one needs a theoretical model that meets the following requirements [1]:

- It should respect the main physical conservation laws.
- It should permit a genuine treatment of the global toroidal geometry.
- It should have a decent mathematical structure.

Ideal MHD is presently the only model that satisfactorily combines these features. This model treats the plasma as a perfectly conducting fluid interacting with a magnetic field. It is interesting to notice that all modern physics seems to have been eliminated from this theory: No quantum effects are taken into account, neither are relativistic corrections considered, all kinetic effects have been removed by averaging over the velocity distributions of the individual particles, even electromagnetic waves have been eliminated by the neglect of the displacement current, and, finally, the model is considered to be ideal, i.e., without dissipation. Nevertheless, ideal MHD represents the simplest physical theory that still makes sense in the context of plasma confinement

for CTR.

2.3. Equations of Ideal MHD

The equations of ideal MHD may be written as follows:

$$\rho \frac{d\boldsymbol{v}}{dt} = -\nabla p + (\nabla \times \boldsymbol{B}) \times \boldsymbol{B}, \tag{4}$$

$$\frac{\partial \boldsymbol{B}}{\partial t} = \nabla \times (\boldsymbol{v} \times \boldsymbol{B}), \tag{5}$$

$$\frac{\partial p}{\partial t} = -\boldsymbol{v} \cdot \nabla p - \gamma p \nabla \cdot \boldsymbol{v}, \tag{6}$$

$$\frac{\partial \rho}{\partial t} = -\nabla \cdot (\rho \boldsymbol{v}). \tag{7}$$

Here, ρ is the density, $\boldsymbol{v}$ is the velocity, p is the pressure, and $\boldsymbol{B}$ is the magnetic field. These four equations with associated initial data and boundary conditions, together with a specification of the geometry (as in Fig. 2), constitute the most global approach to the description of confinement problems in CTR.

Concerning the three requirements for an acceptable model mentioned above, we notice that Eqs. (4)–(7) express the conservation of momentum, magnetic flux, entropy, and mass, respectively. It has been established by Friedrichs [7] that these equations constitute a system of nonlinear symmetric hyperbolic partial differential equations, where the nonlinearity is only of a quasilinear nature. Consequently, this set of equations is well-suited for numerical solution as an initial value problem for toroidal geometries [8–10].

If we wish to study plasma–vacuum systems with an interface (Fig. 1) we need to supplement Eqs. (4)–(7) with the equations describing the vacuum magnetic field $\hat{\boldsymbol{B}}$:

$$\nabla \times \hat{\boldsymbol{B}} = 0, \tag{8}$$

$$\nabla \cdot \hat{\boldsymbol{B}} = 0. \tag{9}$$

These equations are all that is left from Maxwell's equations when the displacement current is negligible. The plasma variables ρ, p, $\boldsymbol{v}$, $\boldsymbol{B}$ are connected with the vacuum variable $\hat{\boldsymbol{B}}$ through two boundary conditions:

$$\boldsymbol{n} \cdot \boldsymbol{B} = \boldsymbol{n} \cdot \hat{\boldsymbol{B}} = 0, \tag{10}$$

$$[\![p + \frac{1}{2} B^2]\!] = 0, \tag{11}$$

which guarantee that $\boldsymbol{B}$ and $\hat{\boldsymbol{B}}$ remain tangential to the plasma vacuum interface and that the total pressure is continuous across this interface. The discontinuity of the tangential component of $\boldsymbol{B}$, which is allowed by Eqs. (10) and (11), is thought to originate from a surface current flowing at the plasma surface:

$$\hat{\boldsymbol{j}} = \boldsymbol{n} \times [\![\boldsymbol{B}]\!]. \tag{12}$$

Finally, the whole configuration is either closed off from the outside world by the presence of a perfectly conducting wall where $\boldsymbol{n} \cdot \hat{\boldsymbol{B}} = 0$ or it is open with respect to a set of coils which feed in energy and flux. In the present paper we will be exclusively concerned about the first possibility.

3. Two Approaches

3.1. Global Interface Problems: Rayleigh–Taylor and Kink Instabilities

Two typical interface problems that are relevant to the stability of plasmas confined by magnetic fields are shown in Fig. 4: The Rayleigh–Taylor instability of a gravitating plasma slab embedded in a magnetic field which abruptly changes direction at the plasma–vacuum interface (Fig. 4a) and the kink instability of a straight plasma cylinder with a longitudinal magnetic field and surrounded by a helical magnetic field in the vacuum (Fig. 4b). The two situations are quite similar and represent just a minor modification of the two examples that were first investigated by Kruskal and Schwarzschild [11].

In both cases the change of direction of the magnetic field at the plasma–vacuum interface is caused by perpendicular surface currents. These currents also create a jump in the magnitude of $\boldsymbol{B}$ which, according to Eq. (11), allows for a finite value of β of the confined plasma: $\beta \equiv 2p/\hat{B}^2 = [\![B^2]\!]/\hat{B}^2$.

To analyze the stability of these configurations the static equilibrium is subjected to a small perturbation of the form

$$\xi(x)e^{i(\boldsymbol{k}\cdot\boldsymbol{r}-\omega t)}, \tag{13}$$

where x is the direction of inhomogeneity (r for the cylindrical case) and $\boldsymbol{k}$ is the wavevector in the two homogeneous directions: $(0, k_y, k_z)$ for the slab and $(m/r, 0, k)$ for the cylinder. Exploiting the equations of Sec. 2, a straightforward analysis leads to ordinary second order differential equations of the normal components of $\boldsymbol{v} = \partial\boldsymbol{\xi}/\partial t$ in the plasma and of the perturbation $\hat{\boldsymbol{Q}}$ of the vacuum magnetic field. Satisfying the appropriate boundary conditions then leads to the following dispersion equation for long-wavelength perturbations:

$$\rho\omega^2 = (\boldsymbol{k}\cdot\boldsymbol{B})^2 + (\boldsymbol{k}\cdot\hat{\boldsymbol{B}})^2 - \begin{cases} k^2\rho g a & \text{for the slab} \\ |m|\hat{B}_0^2/a & \text{for the cylinder.} \end{cases} \tag{14}$$

Equation (14) is a typical example of the kind of results one obtains from a global analysis like the one we have just described. There are three terms which may be associated with the perturbation of the plasma, of the vacuum, and of the plasma–vacuum interface, respectively. Here, the first two terms, which are positive, are the stabilizing contributions due to the bending of the plasma and vacuum magnetic field lines. The third term, which is negative, is the term responsible for the Rayleigh–Taylor instability of the slab or the kink instability of the cylinder.

Although the driving mechanisms of the two instabilities are different (gravity in the first and curvature of the magnetic file lines in the second case), the magnitude of the unstable term is determined in both cases by the amount of surface currents flowing at the plasma–vacuum interface. Thus, the parameter β enters into the calculation as a parameter associated with instability. On the other hand, it is clear from the form of Eq. (14) that the instability is counteracted by shear of the magnetic field, i.e., by the change of direction of the field lines across the plasma–vacuum interface. This effect prevents the occurrence of perturbations for which both stabilizing terms would vanish simultaneously. Consequently, perturbations for which $\boldsymbol{k} \cdot \boldsymbol{B}$ is minimal ($\boldsymbol{k}$ lying in the shaded area of Fig. 5) still create a finite amount of stabilizing energy.

In Fig. 6 the frequencies of the waves (or the growth rates of the instabilities when $\omega^2 < 0$) are plotted versus the component of the wavevector parallel to the magnetic field in the plasma. Also indicated are the regions corresponding to Fig. 5, where the influence of field–line bending is minimal. From Fig. 6a the destabilizing influence of β is obvious. In Fig. 6b the growth rate of the kink instability is plotted for $\beta = 0$. Clearly, already in the absence of plasma pressure the plasma is violently unstable for a wide range of values of $k_{\|}$. Typically, growth rates of the order of 10^6 $\sec^{-1}$ are obtained from Eq. (14), so that one cannot tolerate these kinds of instabilities in a thermonuclear confinement experiment.

Considering the straight cylinder as the leading order approximation of a toroidal geometry, a very simple stabilization method of the kink instability is found to reside in the quantization condition $k_{\|} = n/R$, where n is the toroidal wave number. Clearly, when the first mode ($n = 1$) has a longitudinal wavelength that does not fit into the torus, one does not have to worry about the kink mode any more. A simple derivation by means of Eq. (14) shows that this is equivalent to the celebrated Kruskal–Shafranov limit,

$$q^* = q(a) > 1, \tag{15}$$

which is a limit on the toroidal plasma current according to Eq. (3).

3.2. Local Phenomena: Characteristics

An entirely different approach to the solution of the equations of Sec. 2 is obtained when one considers the problem form a local point of view. Rather than trying to catch the global structure of the solutions at once, as in Sec. 3.1, one pays more attention to the internal inhomogeneities of the plasma and tries to construct solutions in the large from local constituents. This is the method of characteristics, which is very well described in Refs. [7] and [12].

Along these lines the phase and group diagrams of the MHD waves are obtained from Eqs. (4)–(7) by

perturbation methods. The group diagram (Fig. 7a) is obtained by computing the distance which a plane wave front travels along the wavevector $\boldsymbol{k}$ after having passed the origin at $t = 0$. Since the MHD equations comprise both magnetic and acoustic phenomena, two distinctive speeds enter the description, viz. the Alfven speed b and the sound speed c:

$$b \equiv B/\sqrt{\rho}, \quad c \equiv \sqrt{\gamma p/\rho}. \tag{16}$$

The interplay of these phenomena constitutes part of the beauty of ideal MHD. Three waves are obtained: (1)The fast magnetoacoustic wave, which transforms into an ordinary sound wave if the magnetic field vanishes ($b \to 0$), (2) The Alfven wave, which propagates preferentially along the magnetic field; (3) The slow magnetoacoustic wave, which also exhibits a strong anisotropy with respect to the magnetic field.

The actual characteristic surfaces, or rather the spatial parts of them, are obtained by considering the response to a point disturbance emitted at $t = 0$ from the origin, i.e., by constructing the envelopes of all plane waves passing through the origin of Fig. 7a. This gives the group diagram, or ray surface, depicted in Fig. 7b. Notice that the anisotropy is even more pronounced now, with the Alfven waves moving as two points ($\pm b$) and the slow waves as two cusped figures in opposite directions along the magnetic field.

The three MHD waves are most easily distinguished on the basis of their polarizations, which are shown in Fig. 8. The Alfven waves are characterized by a displacement $\boldsymbol{\xi}_A$ and a magnetic perturbation Q_A which are both perpendicular to the plane through $\boldsymbol{k}$ and $\boldsymbol{B}$, whereas the polarizations $\boldsymbol{\xi}_S$ and $\boldsymbol{\xi}_F$ and the magnetic perturbations Q_S and Q_F of the magneto acoustic waves are situated in this plane. Of particular importance is the fact that the three vector $\boldsymbol{\xi}_S$, $\boldsymbol{\xi}_A$ and $\boldsymbol{\xi}_F$ form an orthogonal triad so that arbitrary initial conditions can be decomposed in terms of the three underlying waves.

The method of characteristics consists of solving the nonlinear MHD equations by integrating along the characteristics. The overall inhomogeneity of the medium (e.g., due to the toroidal geometry) only enters indirectly through the fact that we propagate the solution from one space–time point to the next. The advantage of this method is that it is general, not restricted to certain specific geometries. An obvious disadvantage as compared to the global approach sketched in Sec. 3.1 is that it is difficult to obtain global solutions this way and that one is quickly led to a large computational effort.

In the next section we will describe a kind of merging of the two approaches, where both the global and the local aspect of the theory are taken seriously, albeit to the cost of losing the nonlinearities.

4. Spectral Theory of Ideal MHD

4.1 Outline

The global analysis of plasma–vacuum systems as exemplified by the two cases treated in Sec. 3.1 has the obvious shortcoming of doing little justice to the internal structure of the plasma equilibrium, as expressed, e.g., by the profiles $\rho(r)$, $p(r)$, $B_\theta(r)$, $B_z(r)$ of the linear pinch. In toroidal geometry these profiles even depend on two coordinates (r, θ or ψ, χ). On the other hand, the method of characteristics indicated in Sec. 3.2 does not permit us to gain much analytical insight into the overall solutions for confined plasmas. Here, the spectral theory of ideal MHD, which has been extensively investigated over the past ten years, suggests itself as the most logical approach for the solution of these problems.

The following questions present themselves: What is the fate of the three ideal MHD waves shown in Fig. 8 when the locally homogeneous background is replaced by the globally inhomogeneous and curved environment of confined plasmas? What is their role in determining the stability of toroidal systems? Significant progress in the solution of these questions has been obtained along three lines: (1) For 1D inhomogeneous plasmas (slab, cylinder) the spectrum has been partly disentangled [13–20]. (2) For 2D inhomogeneous plasmas (axisymmetric torus) analytical progress has been obtained by means of the so–called ballooning representation [21–24]. (3) Numerical results on a wide variety of 2D problems have been produced by means of perfected equilibrium and stability codes, notably PEST and ERATO [25–34]. We will discuss some of these items in the following, while misusing the occasion by adding some new results obtained along the first line (Sec. 4.3) and by turning to a discussion of the program HBT when discussing 2D numerical techniques (Sec. 5).

Spectral theory of ideal MHD starts with the assumption that the plasma motion may be described as a departure from a static equilibrium state, where the plasma is at rest: $\boldsymbol{v}_0 = 0$. While the density, ρ_0, may be chosen arbitrarily, the two other variables p_0 and $\boldsymbol{B}_0$ according to Eq. (4) then have to satisfy the equilibrium equations

$$\begin{aligned} \nabla p_0 &= (\nabla \times \boldsymbol{B}_0) \times \boldsymbol{B}_0, \\ \nabla \cdot \boldsymbol{B}_0 &= 0 \end{aligned} \tag{17}$$

This leads to trivial equations in one dimension, whereas for 2D systems a nonlinear partial differential equation is obtained, the Grad-Shafranov equation.

Perturbations of this equilibrium state are described by the plasma displacement vector $\boldsymbol{\xi}(r, t)$, connected with the velocity by the relation $\boldsymbol{v}_1 = \partial \boldsymbol{\xi} / \partial t$. Inserting this expression into the Eqs. (4)–(7) directly leads to the

famous linearized equation of motion for ideal MHD [35]:

$$\rho_0 \frac{\partial^2 \boldsymbol{\xi}}{\partial t^2} = \underline{\mathcal{F}}(\boldsymbol{\xi}), \tag{18}$$

where

$$\begin{aligned} \underline{\mathcal{F}}(\boldsymbol{\xi}) &\equiv -\nabla p_1 + (\nabla \times \boldsymbol{B}_0) \times \boldsymbol{B}_1 + (\nabla \times \boldsymbol{B}_1) \times \boldsymbol{B}_0, \\ \boldsymbol{B}_1 &= \nabla \times (\boldsymbol{\xi} \times \boldsymbol{B}_0), \\ p_1 &= -\boldsymbol{\xi} \cdot \nabla p_0 - \gamma p_0 \nabla \cdot \boldsymbol{\xi}. \end{aligned} \tag{19}$$

Turning to a study of normal mode solutions $e^{-i\omega t}$, the basic equation for ideal MHD spectral theory is obtained:

$$\underline{\mathcal{F}}(\boldsymbol{\xi}) = -\rho\omega^2 \boldsymbol{\xi}, \tag{20}$$

where $\underline{\mathcal{F}}$ is a Hermitian operator. Inserting a particular equilibrium solution of Eq. (17), we may obtain the waves ($\omega^2 > 0$) and instabilities ($\omega^2 < 0$) of the system by solving Eq. (20) subject to certain boundary conditions which may be found in the literature [35].

4.2. 1D Inhomogeneous Plasmas: Gravitating Slab

Let us now reconsider the Rayleigh–Taylor problem of Sec. 3.1, where we eliminate the vacuum region and concentrate the study on the diffuse plasma. According to Eq. (17), supplemented with a gravitational term, the variables $\rho_0(x)$, $p_0(x)$, and $\boldsymbol{B}_0(x)$ should satisfy the equilibrium condition

$$(p_0 + \frac{1}{2} B_0^2)' + \rho_0 g = 0, \tag{21}$$

which leaves great freedom in the choice of equilibrium profiles. In particular, we may choose a field $\boldsymbol{B}_0 = B_y(x)\boldsymbol{e}_y + B_z(x)\boldsymbol{e}_z$ which arbitrarily changes direction when we move in the direction of inhomogeneity, i.e., along the x–axis.

Because inhomogeneities are restricted to x, we may write

$$\xi(r, t) = \xi(x) \exp[i(k_y y + k_z z - \omega t)]. \tag{22}$$

It is now expedient to introduce a projection for the perturbations and the gradient operator which distinguishes between the directions (1) normal to the magnetic surfaces in the direction of the inhomogeneity (unit vector e_n), (2) tangential to the magnetic surfaces and perpendicular to B_0 (unit vector $e_\perp$), and (3) parallel to B_0 (unit vector $e_\parallel$) [see Fig. 9]. This produces the following decomposition:

$$\begin{aligned} \xi(x) &= (X, Y, Z), \\ \nabla &= (\hat{D}, \hat{G}, \hat{F}), \end{aligned} \tag{23}$$

where $\hat{D} \equiv d/dx$, $\hat{G} \equiv k_\perp(x)$, $\hat{F} \equiv k_\parallel(x)$. Using this projection, Eq. (20) becomes

$$\begin{matrix} \hat{D}(\gamma p + B^2)\hat{D} - \hat{F}B^2\hat{F} & [\hat{D}(\gamma p + B^2) + \rho g]\hat{G} & [\hat{D}\gamma p + \rho g]\hat{F} & X & & X \\ -\hat{G}[(\gamma p + B^2)\hat{D} - \rho g] & -\hat{G}(\gamma p + B^2)\hat{G} - \hat{F}B^2\hat{F} & -\hat{G}\gamma p\hat{F} & Y & = -\rho\omega^2 & Y, \\ -\hat{F}[\gamma p\hat{D} - \rho g] & -\hat{F}\gamma p\hat{G} & -\hat{F}\gamma p\hat{F} & Z & & Z \end{matrix} \tag{24}$$

which is the basic equation for the study of the spectrum of a 1D gravitational slab. This system of equations turns out to be equivalent to one ordinary second order differential equation for X [Eq. (28) below], which may be solved subject to the boundary conditions $X = 0$ at $x = 0$ and $x = a$, say. For $g = 0$ and $d/dx = ik_x$, we recover the three waves of Fig. 8.

The first effect of the inhomogeneity is the appearance of two continuous spectra, corresponding to the existence of singular perturbations that are localized on particular magnetic surfaces. These may be found from Eq. (24) by taking the limit $d/dx \to \infty$. In this limit the first component of Eq. (24) may be integrated once to give

$$(\gamma p + B^2)dX/dx \approx -\hat{G}(\gamma p + B^2)Y - \hat{F}\gamma pZ. \tag{25}$$

Redefine: $F \equiv B\hat{F}$ and $G = B\hat{G}$. Inserting expression (25) into the second component of Eq. (24) then yields

$$(\rho\omega^2 - F^2)Y \approx 0, \tag{26}$$

having the solution $Y \approx \delta(x - x_A)$, where $x = x_A$ is the singular point where $\omega^2 = \omega_A^2 \equiv F^2/\rho$. The collection of improper eigenvalues $\{\omega_A^2\}$ for the interval $0 \leq x \leq a$ constitutes the continuous Alfven spectrum. Similarly, inserting the expression (25) into the third component of Eq. (24) gives:

$$\left(\rho\omega^2 - \frac{\gamma p}{\gamma p + B^2}F^2\right)Z \approx 0, \tag{27}$$

having the solution $Z \approx \delta(x - x_S)$, where $x = x_S$ is the singular point where $\omega^2 = \omega_S^2 \equiv [\gamma p/(\gamma p + B^2)]F^2/\rho$. The collection of improper eigenvalues $\{\omega_S^2\}$ constitutes the continuous slow wave spectrum.

In order to go beyond these singular continuum modes, which are extremely localized perturbations, we need to solve the differential equations (24) on a global scale. This is most conveniently done by means of the single second order differential equation for X, which is obtained from Eq. (24) by eliminating Y and Z:

$$\frac{d}{dx}\frac{N}{D}\frac{dX}{dx} + \left[\rho\omega^2 - F^2 + \rho' g - \frac{k^2\rho^2 g^2(\rho\omega^2 - F^2)}{D} + \left\{\rho g \frac{\rho\omega^2(\rho\omega^2 - F^2)}{D}\right\}'\right]X = 0, \qquad (28)$$

where

$$N \equiv \rho^2(\gamma p + B^2)(\omega^2 - \omega_A^2)(\omega^2 - \omega_S^2), \qquad (29)$$

$$D \equiv \rho^2(\omega^2 - \omega_I^2)(\omega^2 - \omega_{II}^2),$$

$$\rho\omega_{I,II}^2 \equiv \frac{1}{2}k^2(\gamma p + B^2)\left[1 \pm \sqrt{1 - 4\frac{\gamma p F^2}{k^2(\gamma p + B^2)^2}}\right]. \qquad (30)$$

Notice that the Alfven and slow mode singularities of Eqs. (26) and (27) now appear as the zeros of the coefficient N in Eq. (28). In addition, two more special frequencies ω_I^2 and ω_{II}^2 appear, which were originally thought to be associated with two more continua [13], subsequently proved to be apparent singularities [14], and finally shown to represent regions of non-monotonicity of the discrete spectrum [15]. For a more extensive derivation of Eqs. (28), see Ref. [36].

One, admittedly somewhat primitive, motive behind this explicit derivation is to impress the reader with the complexity of the basic MHD equations for even the simplest cases. Consider, e.g., the comparable equation for 1D quantum mechanical systems:

$$\left[-\frac{\hbar^2}{2m}\nabla^2 + V(r)\right]\psi = E\psi, \qquad (31)$$

where the gradient operator may still be reduced with respect to the two ignorable coordinates, corresponding to quantum numbers l and m, say. For given l and m, the eigenvalue E of the Hamiltonian operator is then a function of n, the number of nodes of $\psi(r)$. Since Eq. (31) is of a classical Sturm–Liouville type, this dependence is monotonic, so that the schematic representation of Fig. 10 is obtained for the spectrum.

In contrast, the presence of the factor N/D in Eq. (28) points to the fact that the ideal MHD problem is not of a classical Sturm–Liouville type. Consequently, for fixed k_y and k_z, the eigenvalue ω^2 of the MHD force operator $\mathcal{F}$ is not a monotonic function of the number of nodes of $X(x)$. Instead, partial monotonicity

is obtained for the discrete subspectra separately, as schematically shown in Fig. 11 for the case of weak inhomogeneity. It can be shown [15, 18] that the three ideal MHD waves split into five discrete subspectra which cluster at the tips of the slow and Alfven continua $\{\omega_S^2\}$ and $\{\omega_A^2\}$ and at $\omega^2 = \infty$ for the fast subspectra. Sturmian regions, where $\omega^2(n)$ monotonically increases (indicated by the upward arrows in Fig. 11), and anti-Sturmian regions, where $\omega^2(n)$ monotonically decreases (downward arrows), alternate, where it depends on the sign of N/D which of the two options is realized.

The clear separation of subspectra only obtains when the frequency ranges $\{\omega_S^2\}$, $\{\omega_I^2\}$, $\{\omega_A^2\}$, $\{\omega_{II}^2\}$ do not overlap, i.e., when the inhomogeneities are not too strong. It is not difficult to design situations where the whole positive ω^2-axis is covered with continua so that there are no discrete modes at all. On the other hand, if the inhomogeneities are weak, not all discrete subspectra need to be present. This depends on whether certain conditions on the equilibrium variables are satisfied. E.g., expansion in the neighborhood of the Alfven continuum provides the following expression for the cluster spectrum caused by gravity:

$$\omega^2 \approx \omega_A^2 - \frac{G^2}{q^2 B^2} \frac{\rho' g}{\rho}, \tag{32}$$

where q is the local wave number in the x-direction. Hence, if $\rho' g < 0$ an anti-Sturmian Alfven spectrum is obtained, whereas $\rho' g > 0$ provides a Sturmian Alfven spectrum. It is of interest to notice that only in the latter case the discrete Alfven spectrum may spill over to the negative side of the ω^2-axis. This is associated with the interchange instability of a gravitating slab.

To complete this study would require a systematic numerical investigation of Eq. (28) for all kinds of representative equilibria. Such a study has not yet been undertaken. It is embarrassing to notice that ten years of active research in spectral theory of ideal MHD has not yet resulted in a final classification of the spectrum of even the simplest systems. In particular, the first paper initiating a systematic analysis of MHD spectra from a group-theoretical point of view is yet to be written. [Challenge!]

4.3. 1D Inhomogeneous Plasmas: Diffuse Linear Pinch

For plasma confinement problems the geometry of the diffuse linear pinch is of more intrinsic interest than that of the gravitating slab, although the analysis proceeds along the same lines. The equation analogous to Eq. (28) was first derived by Hain and Lust [37]. Writing $r\xi_r = \chi(r) \exp i(m\theta + kz - \omega t)$ it takes the form

$$(f\chi')' - g\chi = 0, \tag{33}$$

where

$$f = N/(rD),$$

$$g = -\frac{1}{r}(\rho\omega^2 - F^2) + \left(\frac{B_0^2}{r^2}\right)' + \frac{4k^2B_0^2}{r^2D}(B^2\rho\omega^2 - \gamma pF^2) \tag{34}$$

$$-\left\{\frac{2kB_0G}{r^2D}[(\gamma p + B^2)\rho\omega^2 - \gamma pF^2]\right\}',$$

and

$$N = (\rho\omega^2 - F^2)[(\gamma p + B^2)\rho\omega^2 - \gamma pF^2], \tag{35}$$

$$D = \rho^2\omega^4 - (m^2/r^2 + k^2)(\gamma p + B^2)\rho\omega^2 + (m^2/r^2 + k^2)\gamma pF^2,$$

$$F = mB_\theta/r + kB_z,$$

$$G = mB_z/r - kB_\theta. \tag{36}$$

Notice immediately: Although the structure of the equations (28) and (33) is very similar, there is no simple recipe to translate gravity into field-line curvature.

A similar picture as Fig. 11 may be obtained for the spectrum of a weakly inhomogeneous linear pinch, where the frequencies ω_I^2 and ω_{II}^2 occupy a larger portion of the ω^2-axis though because of the singularity m^2/r^2 in the expression for D.

It is of interest to analyze the cluster spectra in a little more detail for this case because of the renewed interest in Alfven wave heating [17, 38, 39] and the discovery of global Alfven modes just below the lower edge of the continuum [40, 41]. To that end, consider the case of weak inhomogeneities where Eq. (33) may be solved by means of a WKB solution. Writing

$$\chi(r) = p(r)\exp[i\int q(r)dr], \tag{37}$$

the expressions $p(r)$ and $q(r)$ are determined by requiring that the solution (37) be correct to leading order in the inhomogeneity. Substitution into Eq. (33) yields

$$p \approx (-fg)^{-1/4}, \quad q \approx (-g/f)^{1/2}, \tag{38}$$

where we have to demand that $q^2L^2 \gg 1$ in order for the WKB approximation to be valid. Here, L is the scale length for the inhomogeneities.

The relation (38) gives a local dispersion equation relating ω^2 and the local radial wave number q:

$$q^2 = -(rD/N)g, \tag{39}$$

which is a quintic in ω^2. [No, this has nothing to do with the fact that the discrete spectrum consists of five subspectra]. This equation may be solved in the neighborhood of the Alfven and slow continua, when these are sufficiently far apart. This gives:

$$\rho\omega^2 \approx F^2 - \frac{1}{q^2}A, \tag{40}$$

$$A \equiv \frac{4k^2B_\theta^2(B^2-\gamma p)}{r^2B^2} - \frac{rG^2}{B^2}\left(\frac{B_\theta^2}{r^2} + \frac{2kB_0B^2}{r^2G}\right)'$$

and

$$\rho\omega^2 \approx \frac{\gamma p}{\gamma p + B^2}F^2 - \frac{1}{q^2}S, \tag{41}$$

$$S \equiv -\left(\frac{\gamma p}{\gamma p + B^2}\right)^2\left[\frac{F^4}{\gamma p + B^2} + \frac{rF^2}{B^2}\left(\frac{B_\theta^2}{r^2}\right)' - \frac{4k^2B_\theta^2}{r^2B^2}(\gamma p + B^2)\right]$$

Consequently, for weakly inhomogeneous plasmas discrete Alfven modes may be found either above the continuum when $A < 0$ or below the continuum when $A > 0$. Likewise, anti–Sturmian slow modes are found above the slow continuum when $S < 0$ and Sturmian slow modes are found below the slow continuum when $S > 0$.

Very similar results are obtained from a Frobenius expansion around extrema of the functions $\omega_A^2(r)$ and $\omega_S^2(r)$, as indicated in Fig. 11. Here, there is no restriction on the strength of the inhomogeneities, except that $\{\omega_A^2\}$ and $\{\omega_S^2\}$ should not overlap. We find the following condition for the Alfven continuum to have a clusterpoint from below:

$$\omega_A^{2\prime} = 0, \quad 0 < \frac{1}{8}\rho\omega_A^{2\prime\prime} < A, \tag{42}$$

where A is the same expression as defined in Eq. (40b). Likewise, the condition for the slow continuum to have a clusterpoint from below is found to be

$$\omega_S^{2\prime} = 0, \quad 0 < \frac{1}{8}\rho\omega_s^{2\prime\prime} < S, \tag{43}$$

where S is defined in Eq. (41b). The conditions for the existence of clusterpoints from above are found from the equations (42) and (43) by just reversing both inequality signs.

Since the expressions for A and S involve many free parameters and profile functions it is always possible to find equilibria which satisfy any of the four conditions at some point in the plasma. For such equilibria the general structure of a fully developed spectrum as shown in Fig. 11 is to be expected. In particular, it turns out to be quite easy to satisfy condition (42) for tokamaks, so that Alfven wave heating by resonant excitation of global Alfven modes below the continuum is a viable possibility.

[To my knowledge the conditions (40)–(43), which were announced in Ref. [18] appear here for the first time in the literature.]

4.4. Interface Problems

Returning to the study of plasma–vacuum interface systems it should be clear that the internal structure of the plasma may have a significant influence on the behavior of the global eigenfunctions. On the other hand, the very presence of a discontinuity in the plasma density at the plasma edge also produces a very large effect on the internal modes, even on the continuum modes. This is clear from the expression for the Alfven continuum frequencies $\omega_A^2 \equiv F^2/\rho$, which blows up when $\rho \to 0$. Consequently, a continuum as shown in Fig. 12 is obtained. We have seen that such a continuum with a minimum allows for the excitation of global Alfven modes below the continuum when the condition (42) is satisfied.

Another interesting result of such a radial dependence of $\omega_A^2(r)$ is the fact that the discrete fast wave spectrum is swallowed by the Alfven continuum. Consequently, discrete fast modes do not exist anymore. Instead, one finds modes with eigenfunctions as schematically indicated in Fig. 12b. The interior part of the mode behaves much like an ordinary fast wave, but an Alfven singularity always interferes before it can be joined to the exterior solution, expressed by the vacuum field perturbation $\hat{Q}$. At the singularity the mode necessarily picks up a non–square integrable contribution, both with respect to the potential energy and with respect to the proper norm $I = \frac{1}{2}\int \rho\xi^2 dV$ to be used in MHD spectral studies. The improper part of the eigenfunction may consist both of large contributions, that exhibit a logarithmic behavior of the normal component and a $1/x$ dependence of the tangential component of ξ, and of "small" contributions, that exhibit a jump of the normal component and a δ–function behavior of the tangential component.

Different kinds of improper fast magneto acoustic modes are obtained, depending on the relative amplitude of the "small" and large components. An interesting discrete set of special improper fast modes is obtained when the small contribution does not jump. Such modes are to be considered as the diffuse analogs of the fast surface modes of a sharp–boundary plasma–vacuum system where ρ does not go to zero continuously, but jumps. For the similar case of Alfven surface waves this situation has been analyzed by Tataronis and

Grossmann [42] and by Hasegawa and Chen [43] who have shown, by an analysis adapted from the analogous one for the electrostatic oscillations of an inhomogeneous cold plasma [44, 45], that these quasi–modes exhibit damping due to phase mixing.

With respect to radio frequent heating by means of excitation in the Alfven frequency range, we thus come to the conclusion that both discrete global Alfven waves below the continuum and damped quasi–modes of the fast magneto acoustic spectrum may be excited. A problem to realize here is the very sensitive profile dependence of these two kinds of modes, where the manner in which $\rho \to 0$ at the plasma edge enters in a critical fashion. With respect to the slow continuum modes the situation is even worse since $\omega_S^2 \sim p/\rho$ so that the radial dependence of $\omega_S^2(r)$ at the plasma edge can do almost anything. In particular, one can easily envisage situations where all stable low–frequency discrete modes are swallowed by the slow continuum.

We have derived in Sec. 4.3 conditions for the existence of clusterpoints of the spectrum of the diffuse linear pinch. From the expressions (40) and (41) it is clear that clustering of both Alfven modes (Sturmian and anti–Sturmian) and of the Sturmian slow modes is caused by field line curvature ($B_\theta \neq 0$). So far, we have not mentioned a particularly important kind of clusterpoint, also associated with field line curvature, viz. the one that occurs at marginal stability when we have a point $F \equiv \boldsymbol{k} \cdot \boldsymbol{B} = 0$ in the plasma so that the Alfven and slow continuum have a common minimum at that point: Fig. 13. The condition for such a point to be a clusterpoint is the violation of Suydam's criterion [46] when unstable discrete modes accumulate at $\omega^2 = 0$, i.e., a sufficient condition for instability.

Incidentally, it should be noticed that the mere existence of a point $F = 0$ in a plasma–vacuum system where $\rho \to 0$ continuously at the plasma edge, guarantees that the whole positive ω^2–axis is covered with continua so that stable purely discrete modes no longer exist. Also notice that in this case the continua may fold over onto themselves several times, so that a particularly complicated situation arises.

Let us now return to our discussion of the stability of confined plasmas for CTR purposes. The generalization of Suydam's criterion for a torus is the well–known Mercier criterion [47], which refers to modes that are localized with respect to the field lines at a particular magnetic surface. In the theory of ballooning modes [21–24] a more general kind of localization is considered where also the poloidally localized regions of unfavorable field line curvature can be made to dominate. In the context of the study of the ideal MHD spectrum the discussion of these conditions tends to become quite involved [48]. However, for $\omega^2 < 0$ the spectrum is purely discrete, at least for finite mode numbers. Consequently, if we restrict the study to the question of (in)stability only, we may now move onto the discussion of 2D systems, even though many questions about the spectrum of 1D systems still remain to be solved.

5. 2D Toroidal Confinement Problems

5.1 Outline

In toroidal confinement geometry (see Fig. 2) the solution of the equilibrium itself [Eqs. (17)] becomes a problem. Note that the equations are nonlinear. A very effective method has proven to be the introduction of the poloidal flux function ψ. Since $\nabla \cdot \boldsymbol{B} = 0$, ψ enters as the stream function for the poloidal field:

$$\boldsymbol{B}_p = -\frac{1}{R}\nabla_\perp^* \psi, \quad \text{where} \quad \nabla_\perp^* \equiv (\partial/\partial Z, -\partial/\partial R). \tag{44}$$

Here, R and Z are the coordinates in the poloidal plane: R is the distance from the major axis of the torus and Z is the distance above the equatorial plane. Likewise, since $\nabla \cdot \boldsymbol{j} = 0$, we may introduce a stream function I for the poloidal current:

$$\boldsymbol{j}_p = \frac{1}{R}\nabla_\perp^* I, \quad \text{where} \quad I \equiv RB_\varphi = I(\psi). \tag{45}$$

One also easily shows that $p = p(\psi)$. Consequently, ψ labels the magnetic surfaces, which are tangent to the vectors $\boldsymbol{j}$ and $\boldsymbol{B}$ and orthogonal to the vector ∇p.

The equilibrium problem may be considered as solved if we know $\psi(R, Z)$, since all physical variables are then known in terms of the geometric coordinates R and Z of the poloidal cross-section of the torus. Inserting the expressions (44) and (45) into the force-balance equation $\boldsymbol{j} \times \boldsymbol{B} = \nabla p$ leads to the famous Grad–Shafranov equation:

$$R\frac{\partial}{\partial R}\frac{1}{R}\frac{\partial \psi}{\partial R} + \frac{\partial^2 \psi}{\partial Z^2} = -R^2 p' - II' \qquad (= Rj_\varphi), \tag{46}$$

which should be solved subject to the boundary condition that $\psi = \text{const.}$ at the plasma edge. The physically relevant solutions of Eq. (46) are those that represent a set of nested closed flux contours around a point, the position of the magnetic axis, where $\partial\psi/\partial R = \partial\psi/\partial Z = 0$.

For theoretical analysis it is also convenient to introduce a poloidal angle $\chi(R, Z)$, orthogonal to $\psi(R, Z)$, so that we obtain an orthogonal coordinate system ψ, χ, φ based on the magnetic surfaces. Here, φ is the toroidal angle, which is an ignorable coordinate for the equilibrium. [It should be mentioned that χ is never used in numerical calculations since it misbehaves at the origin when the magnetic surfaces are elliptical. Therefore, other angles are exploited, but we will not go into these details, important as they may be for numerical accuracy.]

The theoretical task posed by the CTR program is to optimize the equilibrium configuration with respect to MHD stability and also to provide a description of the global geometry, including the interaction with the external coils that are needed to create the optimum configuration. Since this problem is too complex to be solved at once, a two–stage procedure is generally followed.

First, the internal problem is considered by itself. One prescribes a certain shape of the cross–section of the plasma and proceeds to solve Eq. (46) and the stability equations. This involves many free parameters and functions: β, q^*, ϵ, shape of the cross–section, and the profiles $p(\psi)$ and $I(\psi)$ [or, equivalently, $q(\psi)$ from Eq. (2)], so that a very efficient solution of Eq. (46) is required to scan parameter space. The internal problem is complete in itself if the plasma is bounded by a perfectly conducting wall of the desired shape. However, if we wish to consider plasma–vacuum interface systems where a wall or a set of coils is situated at a distance from the plasma, the problem becomes ill–posed since small variations in the desired shape of the plasma cross–section will produce large variations of the coil or wall parameters.

The second stage consists of a self–consistent determination of the plasma equilibrium, starting with a prescribed position of the wall or of the coils with prescribed currents. This is the free–boundary problem, which is mathematically well–posed, but significantly harder to solve. Except for the solution of Eq. (46), one now also needs a solution of the vacuum field equations, which is usually obtained by means of Green's function methods, and one needs to match these solutions [through Eqs. (10) and (11)] at an interface whose location is unknown.

From a purely physical point of view the latter procedure might appear to be the correct one, identifying well–posed mathematical problems with physically relevant ones. However, it should be noticed that the actual technological problem is intrinsically ill–posed: Eventually, one is not interested in the purely physical question of a description of the equilibrium and stability of a certain plasma created by certain coils. One is interested in finding out how to produce a plasma with desirable properties (low q^*, high β) by action at a distance, i.e., by external manipulation of the coils and currents. [Accordingly, one should expect the problem of reproducibility and reliability to become a major one in future fusion reactor studies.]

Both fixed–boundary and free–boundary methods have been used extensively in the study of tokamak equilibrium problems [26, 27, 49–54], where Eq. (46) is usually solved by means of some finite difference scheme. Recently, an entirely different approach has presented itself. Starting with the observation that all stability theories are formulated in terms of flux coordinates ψ, χ, φ, one tries to solve the nonlinear equations for the inverse coordinates $R(\psi, \chi)$, $Z(\psi, \chi)$ directly. [Remember: χ should be read here as any poloidal angle]. This eliminates the necessity of having to invert the coordinates in between the equilibrium and stability parts of the numerical calculation. In this method of inverse coordinates or method of moments [55–58] the

solution of the equilibrium problem is reduced to that of solving a set of nonlinear ordinary differential equations for the moments of R and Z. In Sec. 5.2 we will present a third approach to the solution of the equilibrium equations which is based on conformal mapping. In this method the flux function is determined as a function of polar coordinates s, t in a computational plane obtained from the physical plane by conformal mapping. By construction, these coordinates are globally adapted to the geometry of the magnetic surfaces, so that there is no need for coordinate inversion (with one exception, to be mentioned later).

After the equilibrium has been determined with sufficient accuracy, it makes sense to consider the stability problem. The stability of toroidal equilibrium configurations is usually carried out by means of some form of the Rayleigh–Ritz variational principle. Eigenvalues ω^2 of the basic eigenvalue problem (20) are obtained as stationary values of a functional $\Omega^2[\boldsymbol{\xi}]$, the ratio of the potential energy W and the norm I:

$$\delta\Omega^2 = 0, \qquad \Omega^2 \equiv W[\boldsymbol{\xi}]/I[\boldsymbol{\xi}]. \tag{47}$$

Here, $W[\boldsymbol{\xi}]$ is the well–known quadratic form [35] involving the ideal MHD force operator defined in Eq. (19):

$$W = -\frac{1}{2}\int \boldsymbol{\xi}^* \cdot \mathcal{F}(\boldsymbol{\xi}) dV^p = W^p[\boldsymbol{\xi}] + W^s[\xi_n] + W^v[\hat{\boldsymbol{Q}}], \tag{48}$$

where the three expressions to the right refer to the separate contributions of the plasma, of the plasma–vacuum interface, and of the vacuum, respectively. The plasma variable $\boldsymbol{\xi}$ and the vacuum variable $\hat{\boldsymbol{Q}}$ are connected through the boundary condition

$$\boldsymbol{n} \cdot \nabla \times (\boldsymbol{\xi} \times \hat{\boldsymbol{B}}) = \boldsymbol{n} \cdot \hat{\boldsymbol{Q}} \tag{49}$$

at the plasma–vacuum interface, whereas $\boldsymbol{n} \cdot \hat{\boldsymbol{Q}} = 0$ should be posed at the conducting wall surrounding the configuration. The proper norm corresponding to a complete solution of the eigenvalue problem (20) reads:

$$I = \frac{1}{2}\int \rho \boldsymbol{\xi}^* \cdot \boldsymbol{\xi} dV^p. \tag{50}$$

However,r if one is interested in the stability boundaries only, any other convenient norm may be chosen for I.

The global stability problem given by Eqs. (47)–(50) corresponds to a set of linear partial differential equations in the two dimensions ψ and χ when single Fourier components $e^{in\varphi}$ with respect to the ignorable coordinate are considered. This is a problem involving many terms and many parameters. For ballooning modes, localized with respect to a single magnetic surface, a major simplification results since the equations then become ordinary differential equations involving the poloidal angle χ only.

5.2. Conformal Mapping as a Tool for Solving 2D MHD Problems

The global 2D geometry of a toroidal plasma equilibrium is characterized by two important features: (1) the shape of the poloidal cross-section of the plasma–vacuum interface, which we may either prescribe arbitrarily (fixed-boundary problem) or which has to be determined self-consistently (free-boundary problem); (2) the outward shift of the magnetic axis due to finite β.

On the other hand, a fair amount of theoretical insight in ideal MHD stability properties has been gained from 1D straight cylinder theory (cf. Sec. 4.3), i.e., a geometry where the poloidal cross-section of the plasma is a circle with the magnetic axis in the center. The question arises: Is it possible to establish a simple connection between the two pictures?

The Riemann mapping theorem states that a conformal mapping exists which brings about the desired effect: See Fig. 14, which depicts the mapping of an arbitrary curve C (the poloidal cross-section of the plasma) in the z-plane onto a circle C' in the w-plane while mapping the position $z = \delta$ of the magnetic axis onto the origin of the w-plane. A simple example of such a mapping is given by the Moebius transformation:

$$z(w) = (w + \delta)/(1 + \delta w), \tag{51}$$

which maps a circular region onto itself while transforming a point $z = \delta$ into $w = 0$. This simple mapping already provides a transformation which is quite useful in the study of high-β tokamaks with a circular cross-section [59]. Clearly, we need a numerical generalization of such kinds of mappings for arbitrary regions.

The required tool is provided by the recently developed numerical conformal mapping techniques exploiting the fast Hilbert transformation [60]. This very effective method has been successfully applied to the study of the equilibrium and stability of high-β tokamaks [61, 62], which will be discussed in Sec. 6. Since all techniques are extensively described in the mentioned references we will only indicate here the essence of the ideas.

Consider an analytic function $\Omega(w)$ on the unit disk (Fig. 15a):

$$\Omega(w) = \Phi(s,t) + i\psi(s,t), \tag{52}$$

which attains the values $\varphi(t) + i\psi(t)$ at the boundary. The conjugate periodic functions $\varphi(t)$ and $\psi(t)$ then satisfy the Hilbert transformation

$$\varphi(t) = A - \frac{1}{2\pi} \mathcal{P} \int \operatorname{cotg} \frac{1}{2}(t - t')\psi(t')dt'. \tag{53}$$

Indicating the Fourier components of $\varphi(t)$ and $\psi(t)$ as α_m and γ_m, respectively, a discrete representation of this

equation is obtained by taking twice the fast Fourier transformation (FFT):

$$\{\varphi(t_i)\} \quad {}^{FFT-} \quad \{a_m\} \quad {}^{\cdot sg(m)} \quad \{\gamma_m\} \quad {}^{FFT+} \quad \{\psi(t_i)\}. \tag{54}$$

We have termed this algorithm the fast Hilbert transformation (FHT).

The conformal mapping $z(w)$ of a region in the z–plane bounded by a curve C, given by $r = f(\vartheta)$, to the unit disk $w \leq 1$ in the w–plane is obtained by considering the following choice for the analytic function:

$$\Omega(w) \equiv \ln[z(w)/w], \tag{55}$$

which attains the values $\ln f[\vartheta(t)] + i[\vartheta(t) - t]$ at the boundary. Here, $f(\vartheta)$ is known (the curve C), but $\vartheta(t)$ represents the unknown relationship between the angles at the boundary curves in the z– and w–plane, respectively. It follows that $f[\vartheta(t)]$ and $\vartheta(t) - t$ are conjugate periodic functions with respect to each other, satisfying the Hilbert transformation (53). This nonlinear integral equation for the so–called boundary correspondence function $\vartheta(t)$ has been derived by Theodorsen, as long ago as 1931, to study the problem of potential flow around a wing of arbitrary cross–section (Fig. 16a). Its solution becomes nearly trivial by the iterative application of the fast Hilbert transformation given by Eq. (54).

In this manner, an arbitrary shape of the plasma cross–section may be mapped onto a circle. This numerical mapping leaves the position of the origin invariant. A subsequent analytic Moebius transformation of the form (51) then provides the requires final situation where the image of the magnetic axis is situated at the center of the circle.

For the study of discontinuous plasma–vacuum systems we need to be able to treat the vacuum region surrounding the plasma in a similar fashion. This requires the construction of a mapping $z(\omega)$ of a doubly connected region, bounded by two given curves C_0 [given by $r = f_0(\vartheta)$] and C_1 [given by $r = f_1(\vartheta)$] in the z–plane, onto an annulus $p \leq \sigma \leq 1$ in the ω–plane (Fig. 15b). This involves the determination of the two boundary correspondence functions $\vartheta_0(\tau)$ and $\vartheta_1(\tau)$ and of the modulus p, which are obtained from the solution of a pair of nonlinear integral equation. These equations were derived by Garrick, in 1936, to study the problem of potential flow around biplanes (Fig. 16b). The solution of Garrick's integral equations becomes equally simple as that of Theodorsen's equation by the use of the corresponding pair of fast Hilbert transformations, where the number of operations just doubles as compared to that of Eq. (54).

In conclusion: We have effected the simplification of the geometry of a plasma–vacuum system to that of concentric circles (Fig. 16c). The plasma region is mapped onto a disk by means of the internal mapping $z(w)$, which is found in terms of the solution $\vartheta = \vartheta^{in}(t)$ of Theodorsen's integral equation. The vacuum region

is mapped onto an annulus by means of the external mapping $z(\omega)$, which is found in terms of the solution $\vartheta = \vartheta_{0,1}^{ex}(\tau)$ of Garrick's integral equation. In order to connect the physical variables across the plasma–vacuum interface we will have to connect the internal grid with the external one by computing $t = t(\tau)$ or vice versa by computing $\tau = \tau(t)$.

Of course, the construction of the conformal mappings does not solve the physical problem of equilibrium and stability, unless the pertinent equations happen to be the 2D Laplace equation. This is the case for high–β tokamaks with a skin–current when the appropriate ordering is applied (Sec. 6.1). For diffuse high–β tokamaks the equations are more general elliptic partial differential equations so that the mappings do not solve the problem but just facilitate its solution. We will see how in Sec. 6.2.

In closing this section it is appropriate to point out a number of papers of related interest [63–66] concerning the numerical construction of conformal mappings and applications to fluid dynamics. In these papers the problem of severe distortion of boundaries is considered, a problem that becomes urgent in time–dependent studies of fluid interfaces in the nonlinear domain. Here, we have restricted the study to linear perturbations of equilibria that are only moderately distorted, so that these further complications could be avoided.

6. High–β Tokamaks

6.1. Free–boundary High–β Tokamaks with a Skin Current

In Fig. 17a a particular free–boundary equilibrium of a tokamak with skin currents is shown. Equilibrium results here when the outward shift of the plasma column, caused by the finite value of β/ϵ, is balanced by the squeeze of the poloidal flux against the conducting wall. For simplicity the cross–section of the conducting wall has been taken circular and the equilibrium shape $r = f_0(\theta)$ of the plasma cross–sections has been determined self–consistently by solving the free–boundary equilibrium equations in the high–β tokamak ordering. The latter is formally given by

$$\beta \sim \epsilon \ll 1, \quad q^* \sim 1, \quad a\epsilon\beta_p \equiv (\beta/a\epsilon)q^{*2} \sim 1, \tag{56}$$

where

$$\beta_p \equiv 2p/\langle \hat{B}_p \rangle^2$$

[$\sim \epsilon^{-1}$: "high–β_p" would have been a more descriptive term than "high–β"]. The physical meaning of this ordering is that it forces the above–mentioned equilibrium mechanism to appear in the leading order. The method of solution of the free–boundary equilibrium problem may be found in Ref. [62a]. Here, we want to continue our discussion of the previous section, concerning the way in which conformal mapping leads to a complete solution of the stability problem.

Figs. 17b and c show the two mappings that transform the plasma–vacuum geometry in the physical z–plane into the geometry of two concentric circles in the superposed w– and ω–planes. First, a Moebius transformation $z(\zeta)$ is used to map the whole domain, plasma and vacuum region, onto itself. Next, the two numerical mappings $\zeta(w)$ and $\zeta(\omega)$ are used to separately map the internal plasma region onto the disc $s \leq p$ and the external vacuum region onto the annulus $p \leq \sigma \leq 1$. The intermediate Moebius transformation $z(\zeta)$ is somewhat arbitrary since the skin–current plasma has no magnetic axis. We have chosen this mapping for numerical convenience such that the image of the plasma becomes centered with respect to the image of the wall in the auxiliary ζ–plane.

Turning now to the stability analysis, it may be shown [62c] that the high–β tokamak ordering (56) turns both the interior problem for the plasma perturbation $\xi_\perp$ and the exterior problem for the magnetic field perturbation $\hat{Q}_\perp$ into a potential flow problem:

$$\xi_\perp = \nabla^*_\perp \chi, \qquad \Delta_\perp \chi = 0,$$
$$\hat{Q}_\perp = \nabla^*_\perp \hat{\psi}, \qquad \Delta_\perp \hat{\psi} = 0. \tag{57}$$

Consequently, the construction of the two conformal mappings $z(\zeta(w))$ and $z(\zeta(\omega))$ is equivalent to solving these problems. The stream functions χ and $\hat{\psi}$ then need to be connected across the plasma–vacuum interface, which involves the conversion of the internal angle t into the external angle τ.

Through all these simplifications the variational principle (47) may be reduced to the following one–dimensional form for the growth rates of kink modes:

$$\omega^2 = \frac{\oint\oint \xi^*(\tau) N(\tau,\tau') \xi(\tau') d\tau d\tau'}{\oint\oint \xi^*(\tau) D(\tau,\tau') \xi(\tau') d\tau d\tau'}, \tag{58}$$

Here, the kernels N and D are explicit algebraic expressions involving the connection $t(\tau)$ between the internal angle t and the external angle τ, the modus p of the annulus in the ω–plane, the scale factor $H = |dz/d\omega|_0$ of the complete external mapping, and the physical variables $a\epsilon\beta_p$, nq^*, and a. Because the whole problem depends on only these three parameters a complete scan of parameter space can be performed. The resulting stability diagram is shown in Fig. 18.

The whole diagram shown in Fig. 18 may be considered as the high–β generalization of the simple results shown in Fig. 6b, which lead to the Kruskal–Shafranov criterion. Along the nq^* axis two marginal points are found, viz. $nq^* = a^2$ and $nq^* = 1$, i.e., just the usual low–β marginal points in the presence of a conducting wall. [Notice that in Fig. 6b the left marginal point is situated at $nq^* = 0$ since there is no wall assumed in that calculation]. If we increase β the two branches of the marginal curve move toward each other until they close at a certain value of $\beta/a\epsilon n^2$. Above this value complete stability is obtained. Consequently, at sufficiently high β, when the plasma is squeezed against the wall, the Kruskal–Shafranov limit may be surpassed and complete stability is obtained for $\beta > \beta_{min}$. The particular value of β_{min} depends on the magnitude of a, the width of the plasma relative to the radius of the tube. In Fig. 18 the shaded area represents the unstable region for $a = .8$. For that case one obtains $\beta_{min} = .59\epsilon n^2$.

Numerous investigations [67–74] of the fixed–boundary skin–current model with prescribed plasma cross–section have been carried out. A comparison with the present free–boundary calculation shows that the self–consistent shaping of the plasma column by compression against the wall increases the stability significantly, and qualitatively.

6.2. Diffuse High-β Tokamaks

For the skin-current model of a high-β tokamak conformal mappings solve the problem completely. What of more realistic toroidal systems, where the pressure and current profiles are diffuse and, consequently, the equations are no longer the 2D Laplace equations? In this case conformal mappings no longer solve the equations, but they do provide coordinates that are globally adapted to the geometry of the magnetic surfaces. This idea has been implemented in a diffuse toroidal equilibrium and stability code HBT [75].

Although most of the subsequent discussion generalizes to arbitrary diffuse toroidal equilibria, for the purpose of the present review it is most illustrative to restrict the discussion again to the high-β tokamak ordering (56). In that approximation, the Grad-Shafranov equation (46) may be simplified as follows [61]:

$$\Delta_\perp \Psi = A[\Gamma(\Psi) + Bx\Pi(\Psi)] \qquad (= j_\varphi). \tag{59}$$

Here, we have introduced (1) dimensionless coordinates x and y centered at the midpoint of the plasma column, (2) a new dimensionless flux function $\Psi = \psi/\psi_{edge}$ of unit range: $\Psi = 0$ at the magnetic axis ($x = \delta$), $\Psi = 1$ at the plasma edge, (3) unit profiles $\Gamma(\Psi)$ and $\Pi(\Psi)$, related to the profiles $I^{2\prime}$ and p' occurring in Eq. (46): $\Gamma(0) = \Pi(0) = 1$, $\Gamma(1) = \Pi(1) = 0$. Under these conditions A and B become eigenvalues to be determined along with $\Psi(x, y)$.

If we now prescribe the plasma cross-section C and the position of the magnetic axis $x = \delta$ (so that β is to be determined from the solution of Eq. (59) and not the other way around), a conformal mapping $z = z(w)$ as shown in Fig. 14 is determined. This mapping turns Eq. (59) into an equation for $\Psi(s, t)$ where the transformation of the LHS is given by $\Delta_\perp^{(z)} = h^{-2}\Delta_\perp{}^{(w)}$, $h \equiv |dz/dw|$ and the RHS only changes through the introduction of the known function $x = x(s, t)$. Thus, the same structure as Eq. (59) is obtained, but we now have to solve this equation subject to the boundary conditions $\Psi = 0$ at $s = 0$ and $\Psi = 1$ at $s = 1$. Consequently, the flux contours in the w-plane will be near circular, which represents a considerable advantage for the numerics: it speeds up the convergence of the iterative solution of the Grad-Shafranov equation.

In Fig. 19a we show the s, t grids obtained from the solution of Theodorsen's equation and a Moebius transformation for a number of representative plasma cross-sections. The corresponding equilibrium solutions are shown in Fig. 19b for a linear choice of the profiles $\Gamma(\Psi)$ and $\Pi(\Psi)$. The essential point of this figure is the demonstration that the s, t coordinates of the w-plane are very well adapted to the description of the geometry of the magnetic surfaces. Therefore, these coordinates are used throughout the code HBT to compute the equilibrium as well as the stability of diffuse high-β tokamaks.

Once a solution $\Psi(s, t)$ of Eq. (59) is found, a number of different equilibria may be computed from it

through a peculiar scaling of high-β tokamaks. A dimensionless parameter α may be introduced:

$$\alpha \equiv a^2 B_0 / \psi_{edge}, \tag{60}$$

where a is the halfwidth of the plasma column and B_0 is the toroidal magnetic field. This parameter is directly related to $q^* = q^*(a)$ so that we get the equilibria for free if we scan the parameter q^* in a search for the marginally stable points in the $\epsilon\beta_p - nq^*$ diagram (Figs. 20–22).

Through the use of the parameters a, ϵ, a, and B_0 all physical quantities can be made dimensionless and of the order unity. From Eqs. (48) and (50) we then get the following simple expressions for the potential energy W^p of the plasma and the norm I in the high–β tokamak approximation:

$$W = \pi \int\int [|B_p^{-1} F X|^2 + |B_p F Y + 2\kappa_p X|^2 - 2B_p^{-1}(j_\varphi \kappa_p - p'\kappa_t)|X|^2] J d\Psi d\chi,$$
$$I = \pi \int\int [|B_p^{-1} X|^2 + |B_p Y|^2] J d\Psi d\chi. \tag{61}$$

Here, J is the Jacobian of the Ψ, χ, φ coordinates, κ_p and κ_t are the poloidal and toroidal curvatures of the magnetic surfaces:

$$\kappa_p \equiv J^{-1}(JB_p)', \qquad \kappa_t \equiv B_p x', \tag{62}$$

F is the parallel gradient operator:

$$F \equiv -iJ^{-1}\partial/\partial x + na, \tag{63}$$

and X and Y are the normal and perpendicular components of $\boldsymbol{\xi}$:

$$X \equiv B_p \xi_\psi, \qquad Y \equiv iB_p^{-1}\xi_p, \tag{64}$$

which are related through a compressibility relation in the poloidal plane:

$$\partial(JX)/\partial\Psi = i\partial Y/\partial\chi. \tag{65}$$

This latter condition permits us to introduce a stream function S for the perturbations. This, obviously, does not satisfy Laplace's equation in 2D (as in the skin–current case), but it does permit us to express the variational principle for the stability of high–β tokamaks in the form

$$\delta\Omega^2 \equiv 0, \qquad \Omega^2 = W[S]/I[S]. \tag{66}$$

As compared to Eq. (47) this is a significant simplification.

This is the essence of the analysis which has been incorporated in the code HBT, where all functions of Ψ and χ are computed in terms of the coordinates s and t. The formulation also contains the driving forces which are responsible for ballooning modes. Thus, a separate local analysis as in Ref. [23] was carried out and incorporated in HBT [75]. At this point it was necessary to introduce a coordinate inversion in order to be able to localize the modes with respect to a particular magnetic surface. The use of the nonorthogonal coordinates Ψ and t turned out to be the most convenient choice for this purpose.

Finally, we present a number of stability diagrams for high-β tokamaks [75] with a fixed-boundary circular cross-section of the equilibrium in which the wall is moved in from $b/a = 2$ (Fig. 20), to $b/a = 1.25$ (Fig. 21), to $b/a = 1$ (Fig. 2). The curves labeled with different values of σ^2 refer to different σ-stability boundaries [15, 76]. Recall that an equilibrium is called σ-stable if it does not manifest growth of instabilities faster than $\exp(\sigma t)$.

There is a marked difference between stability at low β and at high β, depending on where the wall is situated. When the wall is far away (Fig. 20) increasing β leads to decreased stability for all values of nq^*. When the wall is moved in (Fig. 21) different unstable regions start to separate. In particular if a σ-stability criterion is used it is easier to distinguish different stability regions. E.g., in Fig. 21 a gap between the external and internal kink mode regions appears which is not present if a strict marginal stability criterion ($\sigma^2 = 0$) is exploited. This creates room for a path in parameter space connecting the stable regions at low β with those at high β.

When the wall is close (Fig. 21, 22) several stabilization effects at high β become visible. First, we notice stabilization of the external $m = 1$ kink mode, which we already encountered when discussing the stability of the free-boundary skin-current model (Fig. 18). Next, we encounter a large unstable region of the internal kink mode having both a lower and an upper stability boundary. The lower stability boundary has been known for some time [77, 78], but the upper boundary is of more recent interest [79, 80]: The latter boundary is very similar to the second stability region of localized high-n ballooning modes [81], which has not been indicated in Fig. 21.

With the wall at the plasma (Fig. 22) we found [75] a very striking coincidence of the stability thresholds for internal kink modes and high-n ballooning modes (indicated by the arrow) for a variety of different pressure and current profiles. This suggests that the instability mechanism is quite similar for the two modes. It also lends support for the use of the high-β tokamak ordering leading to the variational principle (66).

7. Perspectives

In the last section we have finally returned to the central questions formulated in Sec. 2.1 concerning the optimization of plasma configurations with respect to the value of β_{crit} for equilibrium and stability. We have purposely taken a long excursion to arrive at that point because this gave us the opportunity to discover some omissions in the development of ideal MHD. One of them was the lack of clarity in the classification of spectral results for simple 1D systems, like the plane gravitating slab and the diffuse linear pinch. If progress would be made there, this would undoubtedly have important implications for the understanding of the more complex 2D systems. One of the problems with a strongly mission–oriented field of research is precisely that these basic questions are never fully solved, due to lack of motivation.

Another omission concerns the development of a nonlinear theory of simple plasma–vacuum interface systems. Again, a number of more sophisticated approaches exist, incorporated in large numerical codes solving the initial–value problem for diffuse 2D and 3D systems, but nothing is known about the nonlinear fate of the gross ideal MHD instabilities in genuine plasma–vacuum interface systems. This may well be explained by the bias of researchers in CTR for plasmas that are diffuse and relatively quiescent, so that the usual split in a static equilibrium state and a small linear perturbation is an adequate picture. Nevertheless, it should be clear that a number of interesting possibilities is eliminated in this manner. E.g., the free–boundary high–β tokamak model discussed in Sec. 6.1 should allow an extension in the nonlinear domain by means of the contour dynamical methods discussed in Ref. [82].

Acknowledgments

The author is indebted to Daniel A. D'Ippolito, Jeffrey Freidberg, Ricardo Galvao, Jan Rem, and Paulo Sakanaka for many years of fruitful interactions.

This work was supported by the U.S. Department of Energy under Contract #DE-AC02-78ET-51013 and by the "Stichting voor Fundamenteel Onderzoek der Materie" (FOM), the "Nederlandse Organisatie voor Zuiver-Wetenschappelijk Onderzoek" (ZWO), and Euratom.

References

[1] J.P. Goedbloed, Lecture Notes on Ideal Magnetohydrodynamics, [Lectures given at Universidade Estadual de Campinas, Brasil, 1978], Rijnhuizen Report 83–145 (1983).

[2] V.D. Shafranov, in Rev. of Plasma Physics 2, ed. by M.A. Leontovich (Consultants Bureau, New York, 1966), 103.

[3] B.B. Kadomtsev, in Rev. of Plasma Physics 2, ed. by M. A. Leontovich (Consultants Bureau, New York, 1966), 153.

[4] J.A. Wesson, Nuclear Fusion 18 (1978) 87.

[5] G. Bateman, MHD Instabilities (MIT Press, Cambridge, 1978).

[6] J.P. Freidberg, Rev. Mod. Phys. 54 (1982) 801.

[7] K.O. Friedrichs and H. Kranzer, Notes on Magnetohydrodynamics VIII. Non Linear Wave Motion (New York University, 1958), NYO–6486.

[8] J.U. Brackbill, in Methods in Computational Physics, ed. J. Killeen (Academic Press, New York, 1976), Vol. 16, 1.

[9] F. Bauer, O. Betancourt, and P. Garabedian, A Computational Method in Plasma Physics (Springer–Verlag, New York, 1978).

[10] A. Schluter and U. Schwenn, Comput. Phys Comm. 24 (1981) 263.

[11] M. Kruskal and M. Schwarzschild, Proc. Roy. Soc. London A223 (1954) 348.

[12] A.I. Akhiezer, I.A. Akhiezer, R.V. Polovin, A.G. Sitenko, and K.N. Stepanov, Plasma Electrodynamics, Vol. I Linear Theory (Pergamon Press, Oxford, 1975).

[13] H. Grad, Proc. Nat. Acad. Sci. 70 (1973) 3277.

[14] K. Appert, D. Berger, and J. Vaclavik, Phys. Fluids 17 (1974) 1471.

[15] J.P. Goedbloed and P.H. Sakanaka, Phys. Fluids 17 (1974) 908.

[16] R.L. Dewar, R.C. Grimm, J.L. Johnson, E.A. Frieman, J.M. Greene, and P.H. Rutherford, Phys. Fluids 17 (1974) 930.

[17] J. Tataronis, J. Plasma Physics 13 (1975) 87.

[18] J.P. Goedbloed, Phys. Fluids 15 (1975) 1090.

[19] Y.P. Pao, Nucl. Fusion 18 (1975) 631.

[20] M.S. Chance, J.M. Greene, R.C. Grimm, and J.L. Johnson, Nucl. Fusion 17 (1977) 65.

[21] B. Coppi, Phys. Rev. Lett. 39 (1977) 939.

[22] D. Dobrott, D.B. Nelson, J.M. Greene, A.H. Glasser, M.S. Chance, and E.A. Frieman, Phys. Rev. Lett. 39

(1977) 943.

[23] J.W. Connor, R.J. Hastie, and J.B. Taylor, Phys. Rev. Lett. 40 (1978) 396; Proc. Roy. Soc. London A365 (1979) 1.

[24] F. Pegoraro and T.J. Schep, Phys. Fluids 24 (1981) 478.

[25] R.L. Dewar, J.M. Greene, R.C. Grimm, and J.L. Johnson, J. Comput. Phys. 18 (1975) 132.

[26] R.C. Grimm, J.M. Greene, and J.L. Johnson, in Methods in Computational Physics, ed. J. Killeen (Academic Press, New York, 1976), Vol. 16, 253.

[27] J.L. Johnson, H.E. Dalhed, J.M. Greene, R.C. Grimm, Y.Y. Hsieh, S.C. Jardin, J. Manickam, M. Okabayashi, R.G. Storer, A.M.M. Todd, D.E. Voss, and K.E. Weimer, J. Comp. Phys. 32 (1979) 212.

[28] A.M.M.Todd, J. Manickam, M. Okabayashi, M.S. Chance, R.C. Grimm, J.M. Greene, and J.L. Johnson, Nucl. Fusion 19 (1979) 743.

[29] L.A. Charlton, R.A. Dory, Y.-K.M. Peng, D.J. Strickler, S.J. Lynch, and D.K. Lee, Phys. Rev. Lett. 43 (1979) 1395.

[30] L.C. Bernard, D. Dobrott, F.J. Helton, R.W. Moore, Nucl. Fusion 20 (1980) 1199.

[31] D. Berger, L.C. Bernard, R. Gruber, and F. Troyon, J. Appl. Math. Phys. (ZAMP) 31 (1980) 113.

[32] W. Kerner, P. Gautier, K. Lackner, W. Schneider, R. Gruber, and F. Troyon, Nucl. Fusion 21 (1981) 1383.

[33] R. Gruber, F. Troyon, D. Berger, L.C. Bernard, S. Rousset, R. Schreiber, W. Kerner, W. Schneider, and K.V. Roberts, Comput. Phys. Commun. 21 (1981) 323.

[34] R.C. Grimm, R.L. Dewar, and J. Manickam, J. Comp. Phys. 49 (1983) 94.

[35] I.B. Bernstein, E.A. Frieman, M.D. Kruskal, and R.M. Kulsrud, Proc. Roy. Soc. London A224 (1958) 1.

[36] J.P. Goedbloed, Physica 53 (1971) 412, 501, 535; Physica 100C (1980) 273.

[37] K. Hain and R. Lust, Z. Naturforsch 13a (1958) 936.

[38] J.A. Tataronis and W. Grossmann, New York University, Courant Institute of Mathematical Sciences, Report C00-3077-102, MF-84 (1977).

[39] A. Hasegawa and C. Uberoi, The Alfven Wave (Technical Information Center, U.S. Dept. of Energy, 1982).

[40] K. Appert, R. Gruber, F. Troyon, and J. Vaclavik, Plasma Phys. 24 (1982) 1147.

[41] S. Mahajan, D.W. Ross, and G.-L. Chen, University of Texas, Report FRCR249 (1982).

[42] J. Tataronis and W. Grossmann, Z. Phys. 261 (1973) 203.

[43] A. Hasegawa and L. Chen, Phys. Rev. Lett. 32 (1974) 454.

[44] E.M. Barston, Ann. Phys. (N.Y.) 29 (1964) 282.

[45] Z. Sedlacek, J. Plasma Phys. 5 (1971) 239.

[46] B.R. Suydam, Proc. of the Second U.N. Intern. Conf. on the Peaceful Uses of Atomic Energy, Geneva, 1958 (Columbia Univ. Press, New York, 1959), Vol. 31, 157.

[47] C. Mercier, Nucl. Fusion 1 (1960) 47.

[48] T.M. Antonsen, A. Ferreira, and J.J. Ramos, Plasma Phys. 4 (1982) 197.

[49] Y. Suzuki, Nucl. Fusion 14 (1974) 345.

[50] K. Lackner, Comput. Phys. Comm. 12 (1976) 33.

[51] R. Teman, Commun. Part. Diff. Eq. 2 (1977) 563.

[52] J. DeLucia, S.C. Jardin, and A.M.M. Todd, J. Comput. Phys. 37 (1980) 183.

[53] J. Blum, J. Le Foll, and B. Thooris, Comput. Phys. Comm. 24 (1981) 235.

[54] T.S. Wang and F.J. Helton, Comput. Phys. Comm. 24 (1981) 255.

[55] P. N. Vabishchevich and L.M. Degtyarev, Dokl. Akad. Nauk 247 (1979) 1342 [Sov. Phys.–Dokl. 24 (1979) 612].

[56] L.L. Lao, S.P. Hirschman, and R.M. Wieland, Phys. Fluids 24 (1981) 1431.

[57] L.E. Zakharov and V.D. Shafranov, in Reviews of Plasma Physics 11 (Energoisdat, Moscow, 1982) 118. [Russian, translation not yet available].

[58] A. Bhattacharjee, J.C. Wiley, and R.L. Dewar, to be published.

[59] J.P. Freidberg and J.P. Goedbloed, in Pulsed High–Beta Plasmas, ed. by D.E. Evans (Pergamon Press, Oxford, 1976), p. 117.

[60] P. Henrici, SIAM Rev. 21 (1979) 481.

[61] J.P. Goedbloed, Comput. Phys. Comm. 24 (1981) 311.

[62] J.P. Goedbloed, Phys. Fluids 25 (1982) 852; 2062; 2073.

[63] B. Fornberg, SIAM J. Sci. Stat. Comput. 1 (1980) 386.

[64] R. Menikoff and C. Zemach, J. Comput. Phys. 36 (1980) 366.

[65] D.I. Meiron and S.A. Orszag, J. Comput. Phys. 40 (1981) 345.

[66] R. Menikoff and C. Zemach, submitted to J. Comput. Phys.

[67] G. Bateman, Phys. Fluids 14 (1971) 1506.

[68] J.P. Freidberg and F.A. Haas, Phys. Fluids 16 (1973) 1909; 17 (1974)) 440.

[69] B.M. Marder, Phys. Fluids 17 (1974)) 447; 639.

[70] J.P. Freidberg and W. Grossmann, Phys. Fluids 18 (1975) 1494.

[71] E. Rebhan and A. Salat, Nucl. Fusion 16 (1976) 805; 17 (1977) 251; 18 (1978) 1639; 20 (1980) 839.

[72] M. Kito and T. Honma, J.Phys. Soc. Jpn. 41 (1976) 1749; Phys. Fluids 21 (1978) 272.

[73] D.A. D'Ippolito, J.P. Freidberg, J.P. Goedbloed, and J. Rem, Phys. Fluids 21 (1978) 1600.

[74] M. Kito, Phys. Fluids 24 (1981) 1142.

[75] R.M.O. Galvao, J.P. Goedbloed, J. Rem, P.H. Sakanaka, T.J. Schep, and M. Venema, Proc. 9^{th} Intern. Conf. on Plasma Physics and Controlled Nuclear Fusion Research, Baltimore (1982) paper P–1–1.

[76] P.H. Sakanaka and J.P. Goedbloed, Phys. Fluids 17 (1974) 919.

[77] M.N. Bussac, R. Pellat, D. Edery, and J.L. Soule, Phys. Rev. Lett. 35 (1975) 1638.

[78] L.E. Zakharov, Fiz. Plasmy 4 (1977) 898 [Sov. J. Plasma Phys. 4 (1978) 503].

[79] S. Tokuda, T. Tsunematsu, M. Azumi, T. Takizuka, and T. Takeda, Nucl. Fusion 22 (1982) 661.

[80] G. B. Crew and J.J. Ramos, Phys. Rev. A26 (1982) 1149.

[81] B. Coppi, A. Ferreira, and J.J. Ramos, Phys. Rev. Lett. 44 (1980)990.

[82] N.J. Zabusky, These Proceedings.

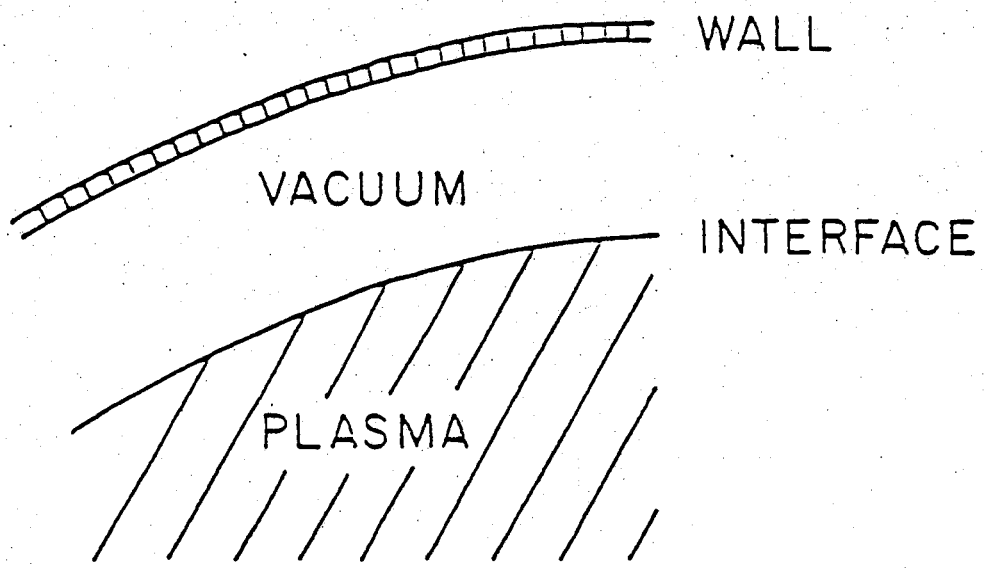

Fig. 1: Plasma–vacuum interface system.

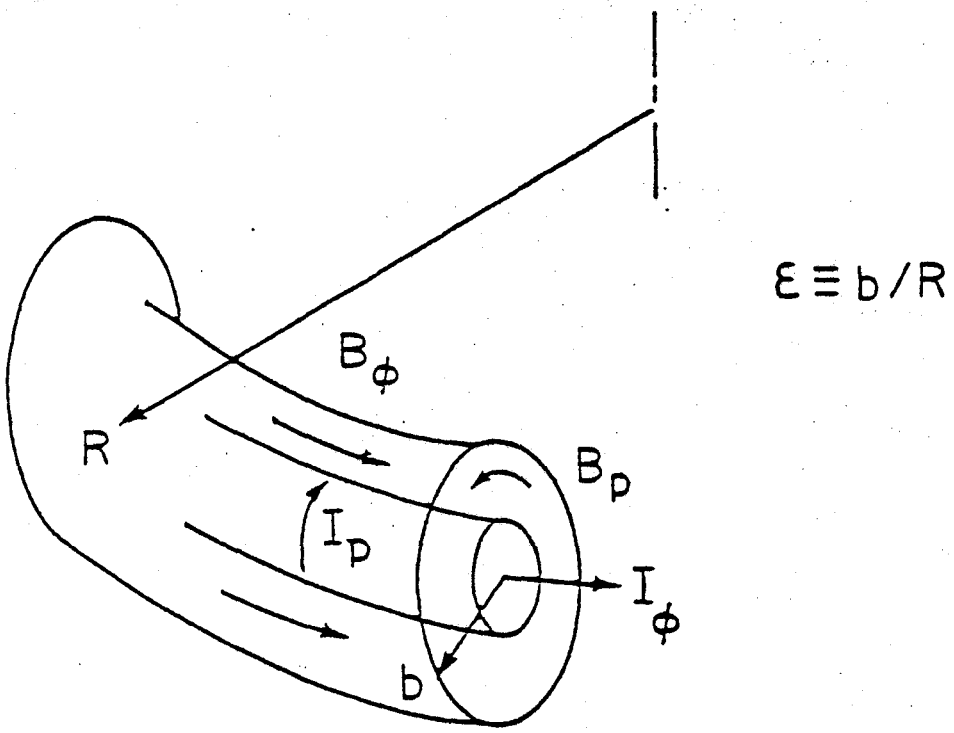

Fig. 2: Toroidal confinement geometry.

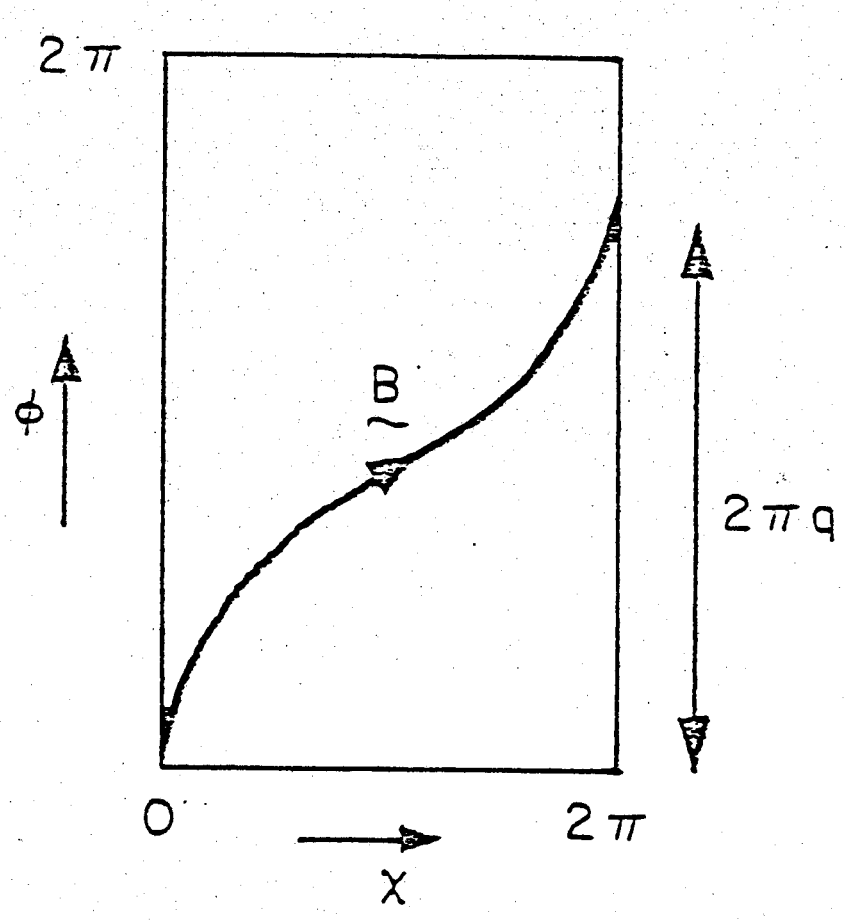

Fig. 3: Field–line topology.

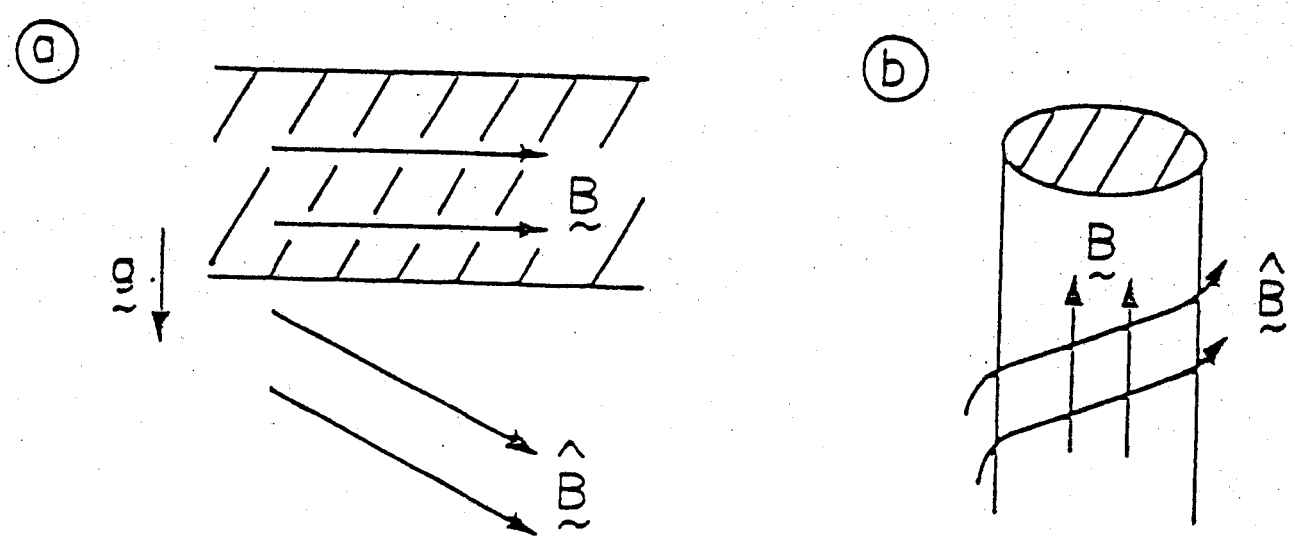

Fig. 4: Geometries for Rayleigh–Taylor and kink instabilities: (a) Gravitating slab. (b)Linear pinch.

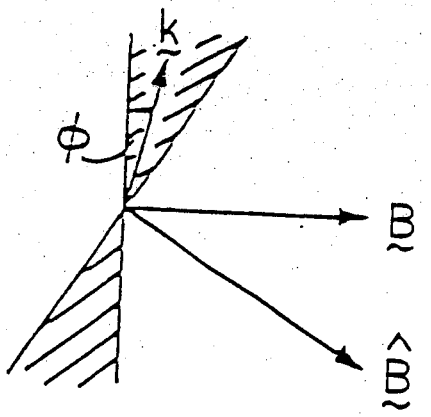

Fig. 5: Direction of k-vector for the most unstable perturbations of the configurations of Fig. 4.

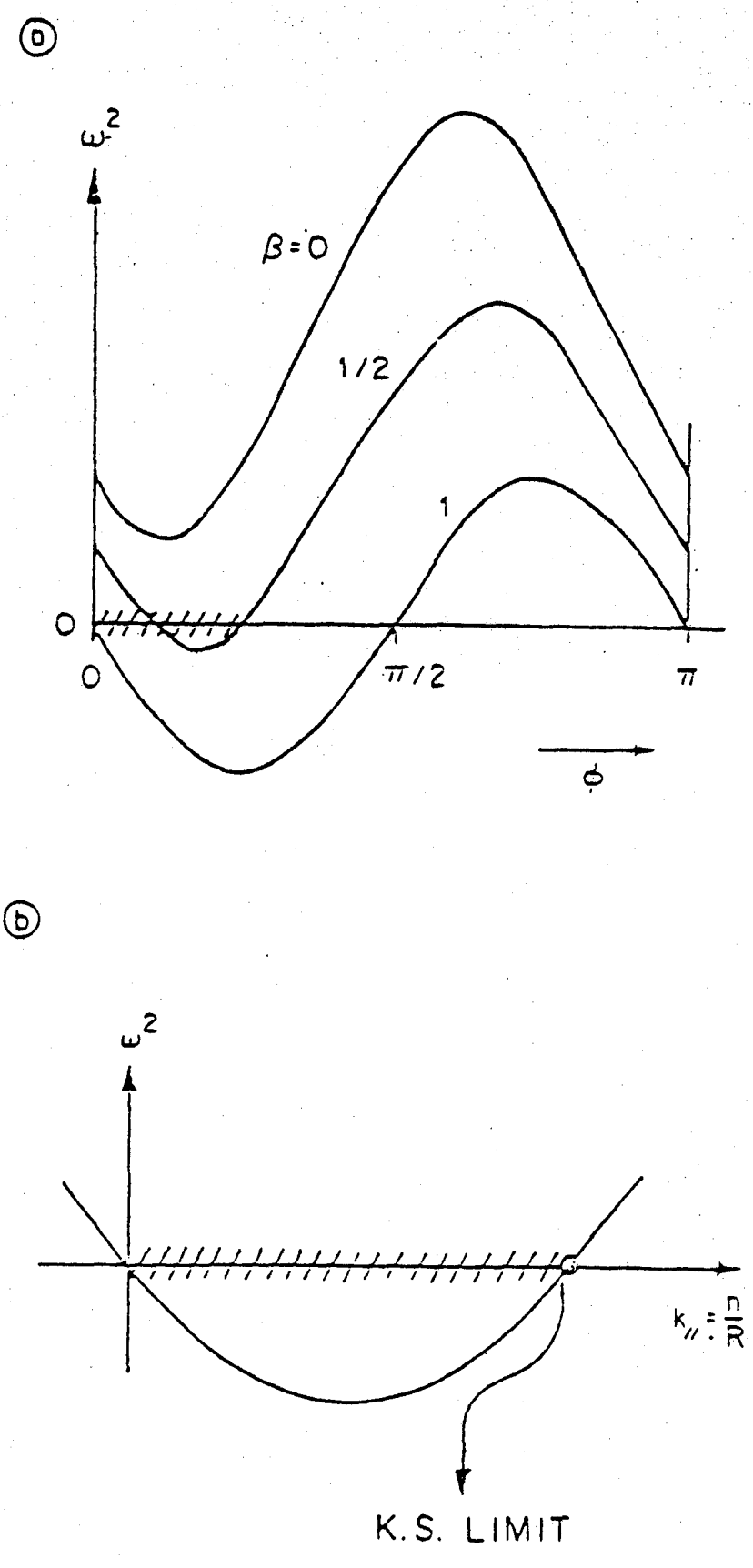

Fig. 6: Stability diagrams for the Rayleigh–Taylor (a) and kink instability (b).

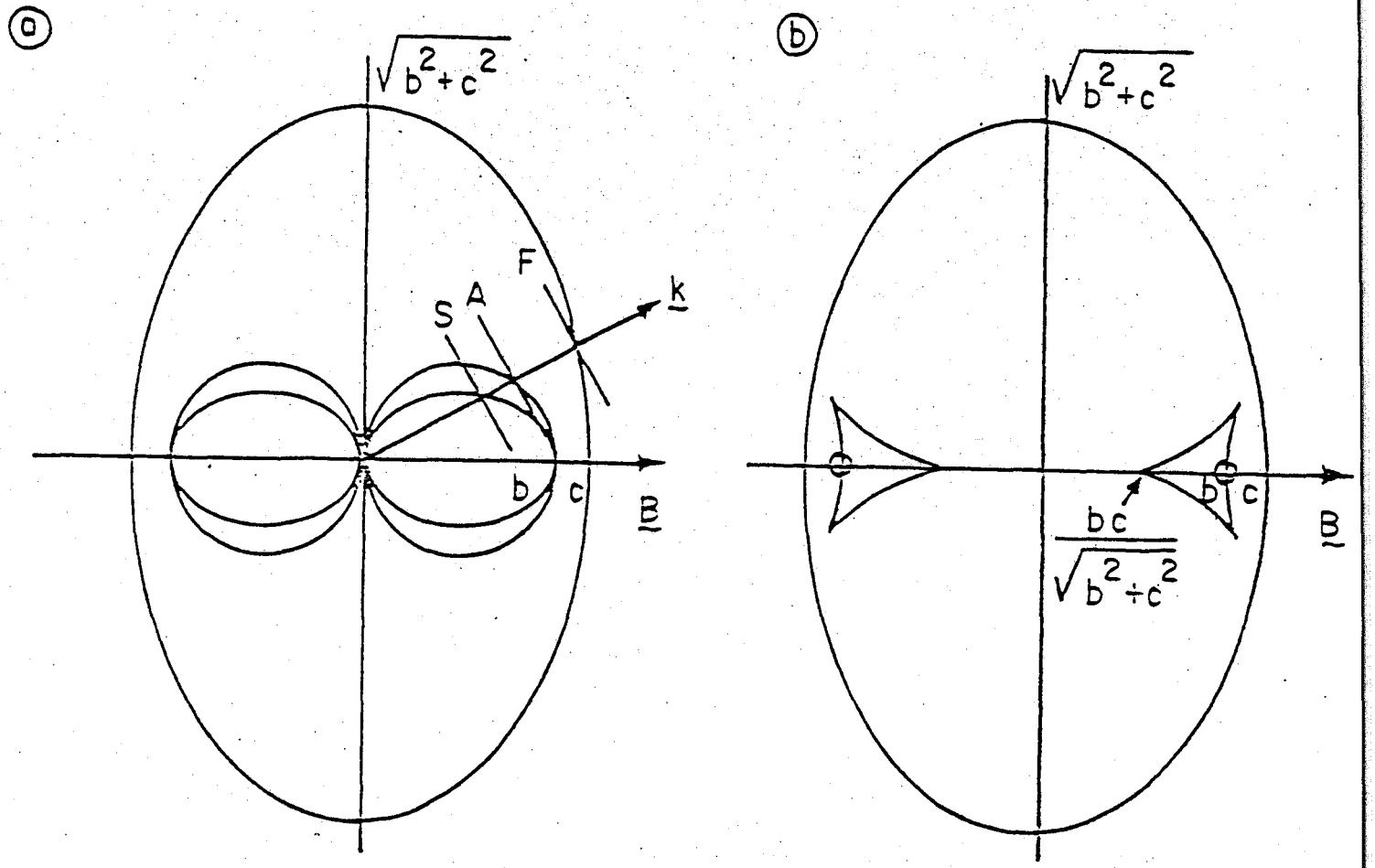

Fig. 7: Phase (a) and group (b) diagrams for the three MHD waves: fast magneto acoustic (F), Alfven (A), and slow magneto acoustic (S). The Alfven speed b is taken smaller than the sound speed *c*.

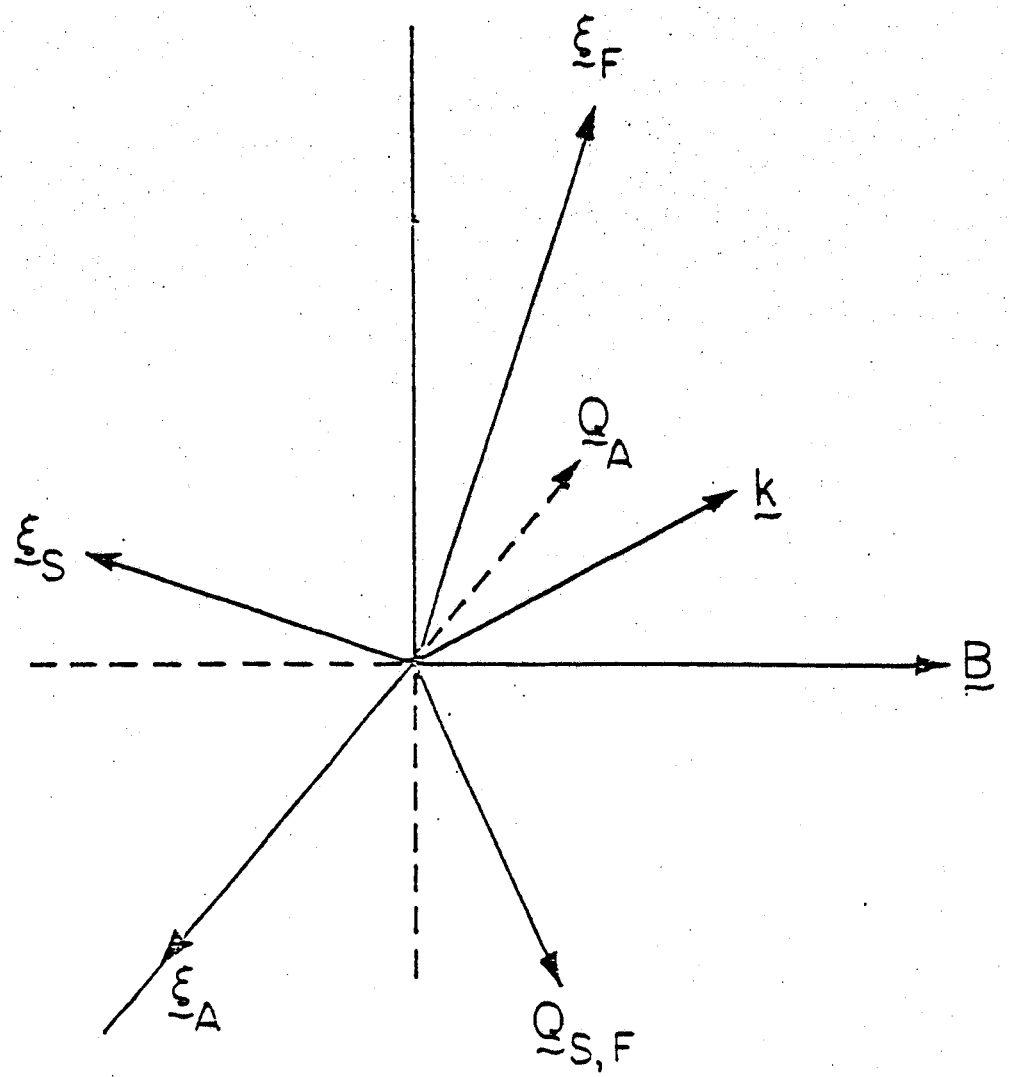

Fig. 8: Displacements ξ and magnetic perturbations Q for the three MHD waves.

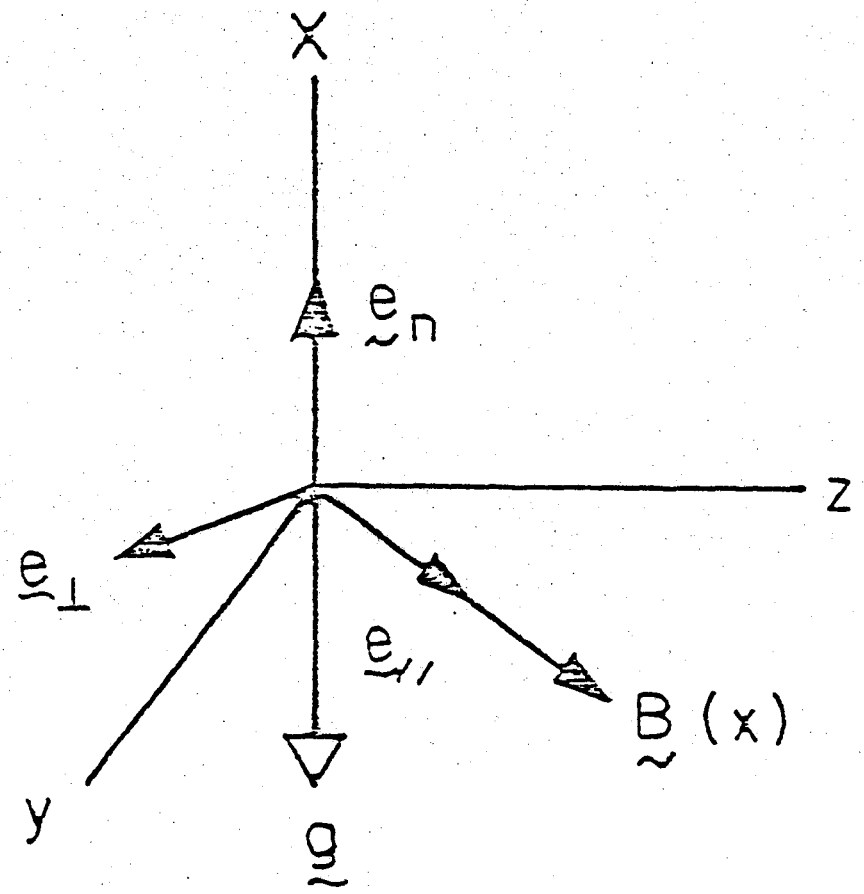

Fig. 9: Projection for inhomogeneous plasmas.

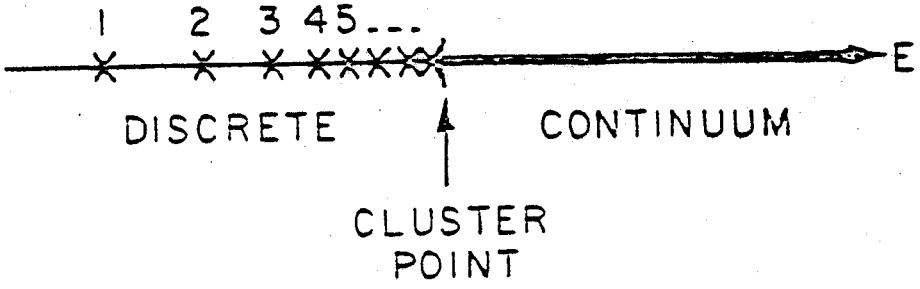

Fig. 10: Structure of the spectrum of a 1D quantum mechanical system.

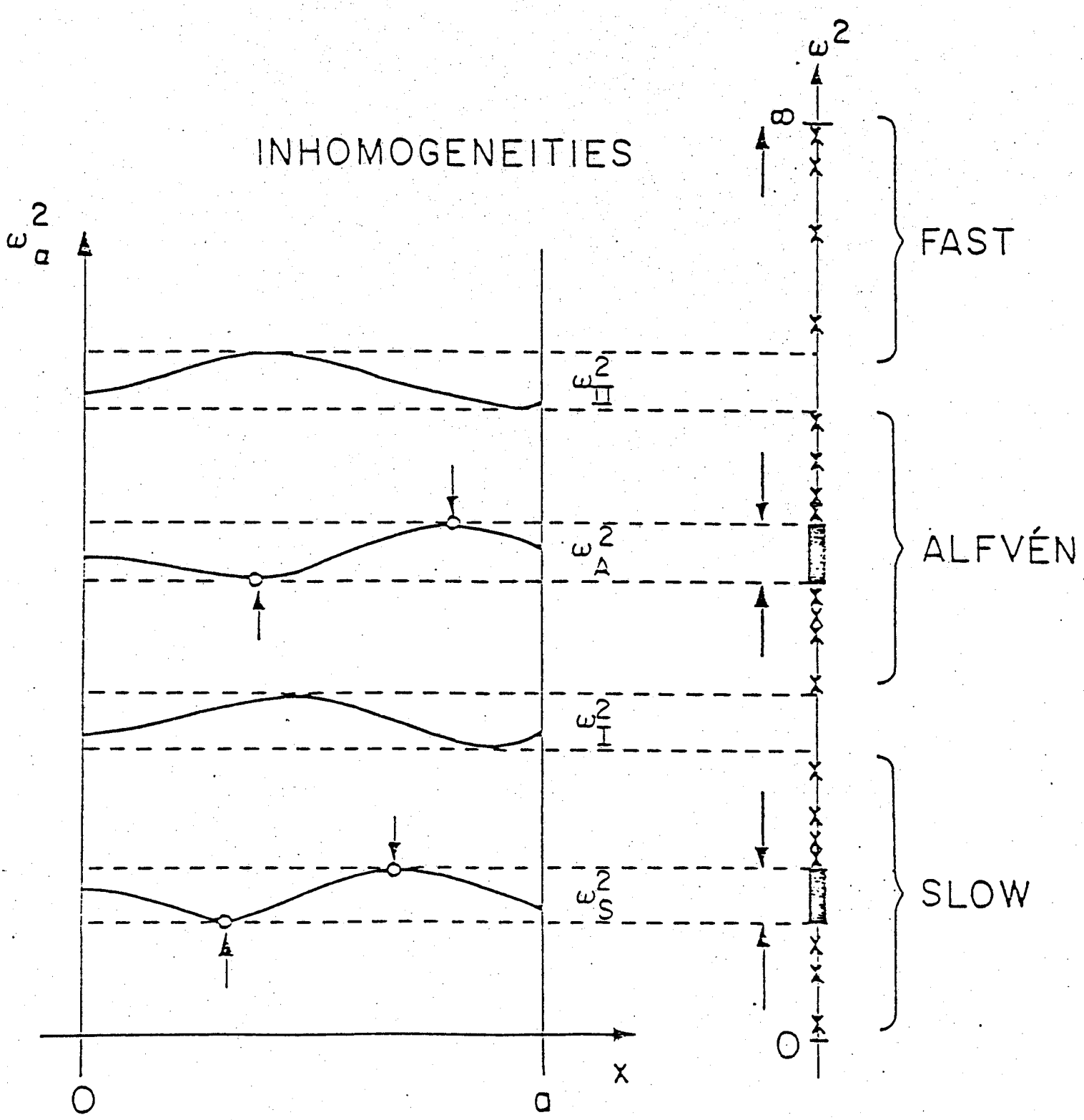

Fig. 11: Structure of the spectrum of a 1D magnetohydrodynamic system. Accumulation of point eigenvalues both from above and below.

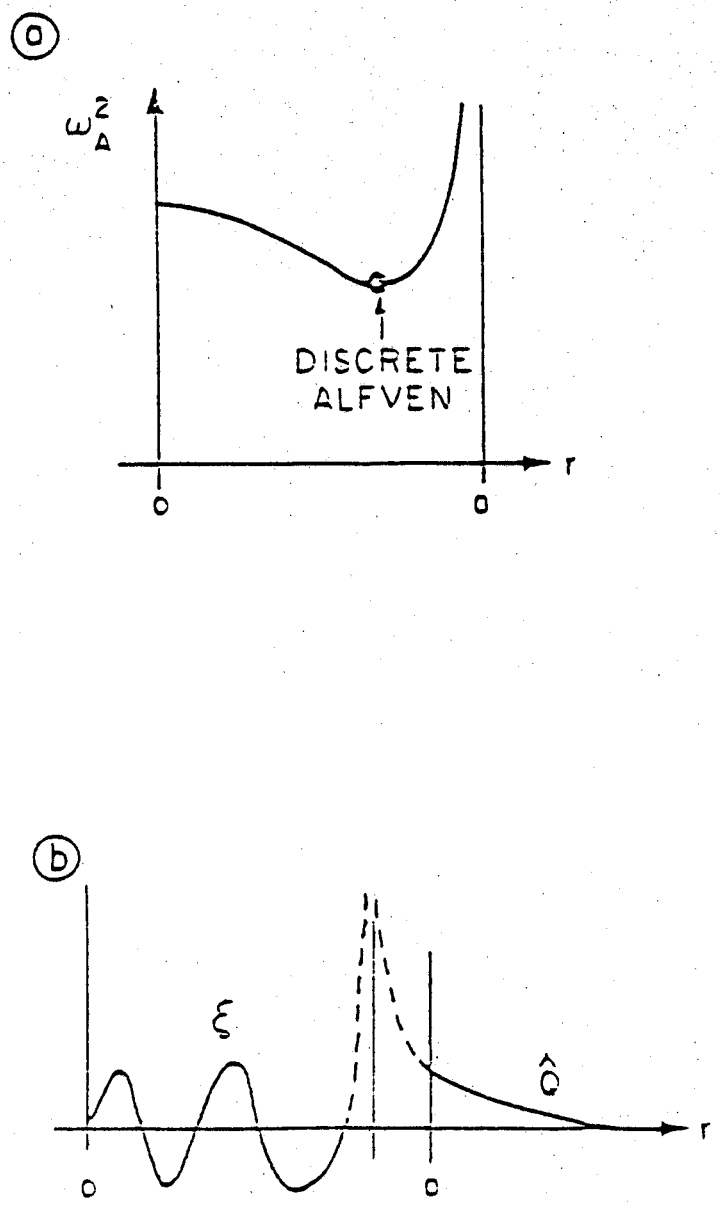

Fig. 12: Typical continuous spectrum of Alfven waves (a) producing a clusterpoint of discrete global Alfven modes and transforming the fast magneto acoustic waves into damped quasi-modes (b).

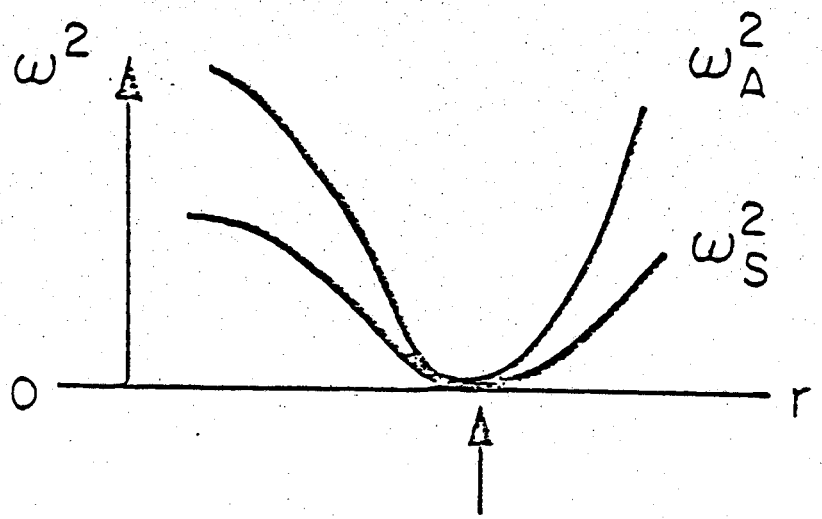

Fig. 13: Clusterpoint of slow magneto acoustic and Alfven modes when Suydam's criterion is violated.

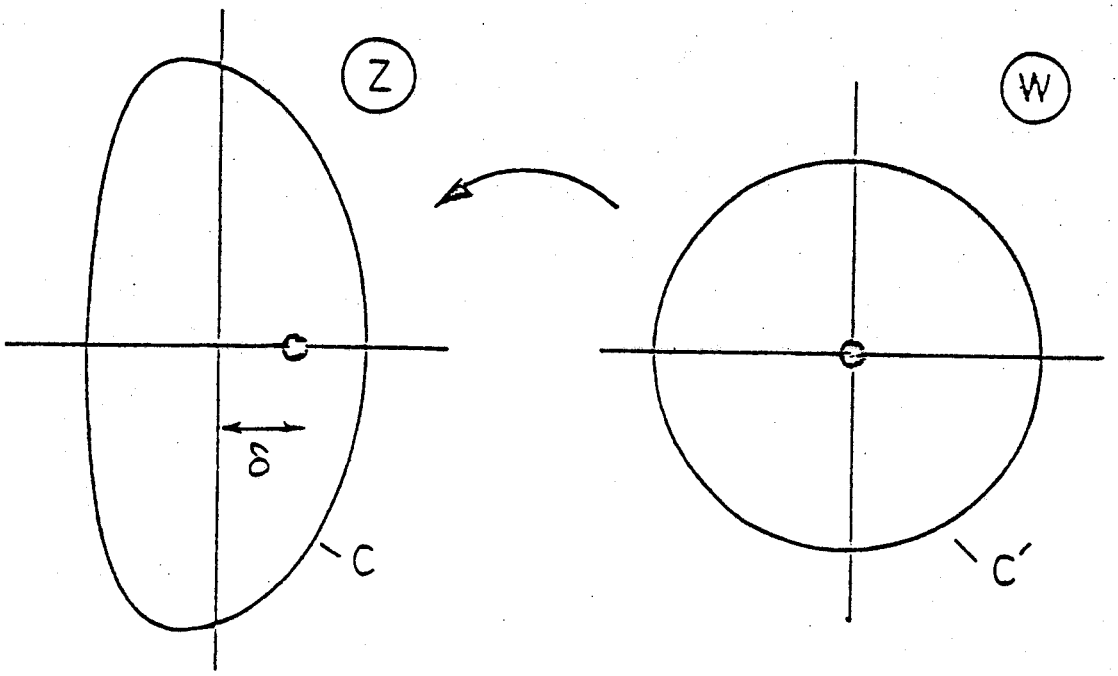

Fig. 14: Conformal mapping of the poloidal cross-section of a toroidal plasma onto a circle with the image of the magnetic axis in the center.

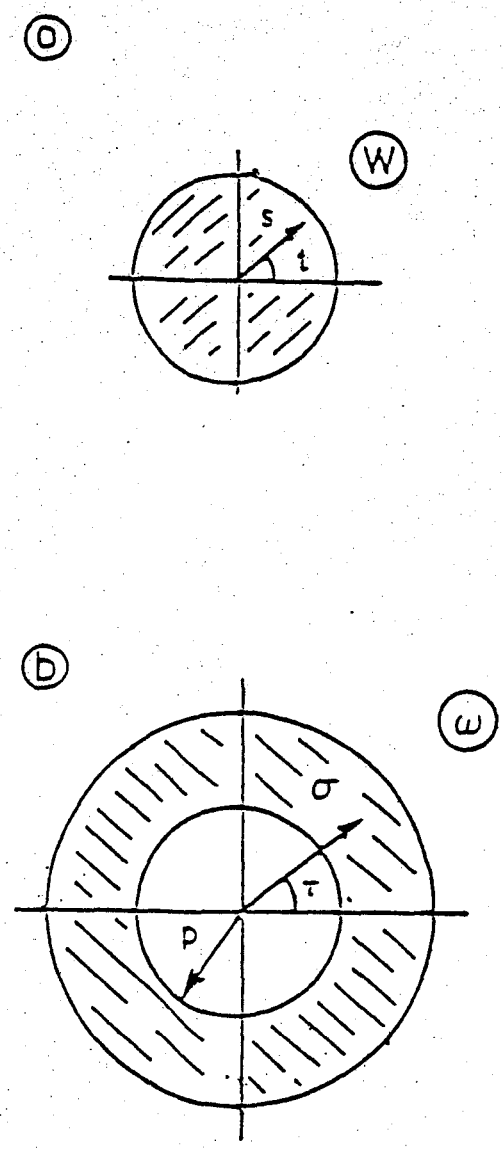

Fig. 15: Domains for the Fast Hilbert Transformation of analytic functions in simply–connected (a) and doubly–connected (b) regions.

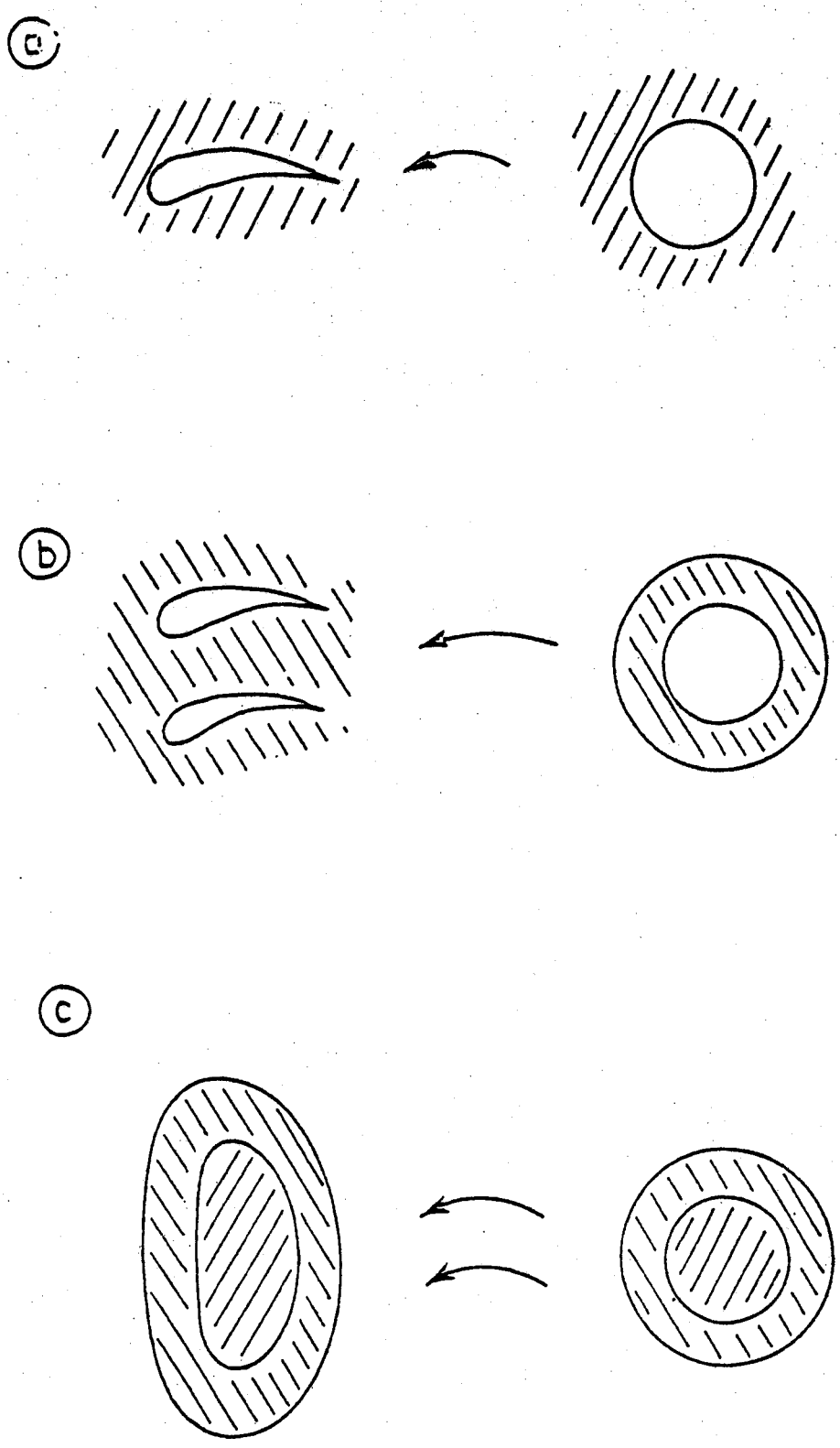

Fig. 16: (a) Theodorsen's mapping of flow around a wing, (b) Garrick's mapping of flow around a biplane, and (c) superposition of the two to describe the stability of tokamaks.

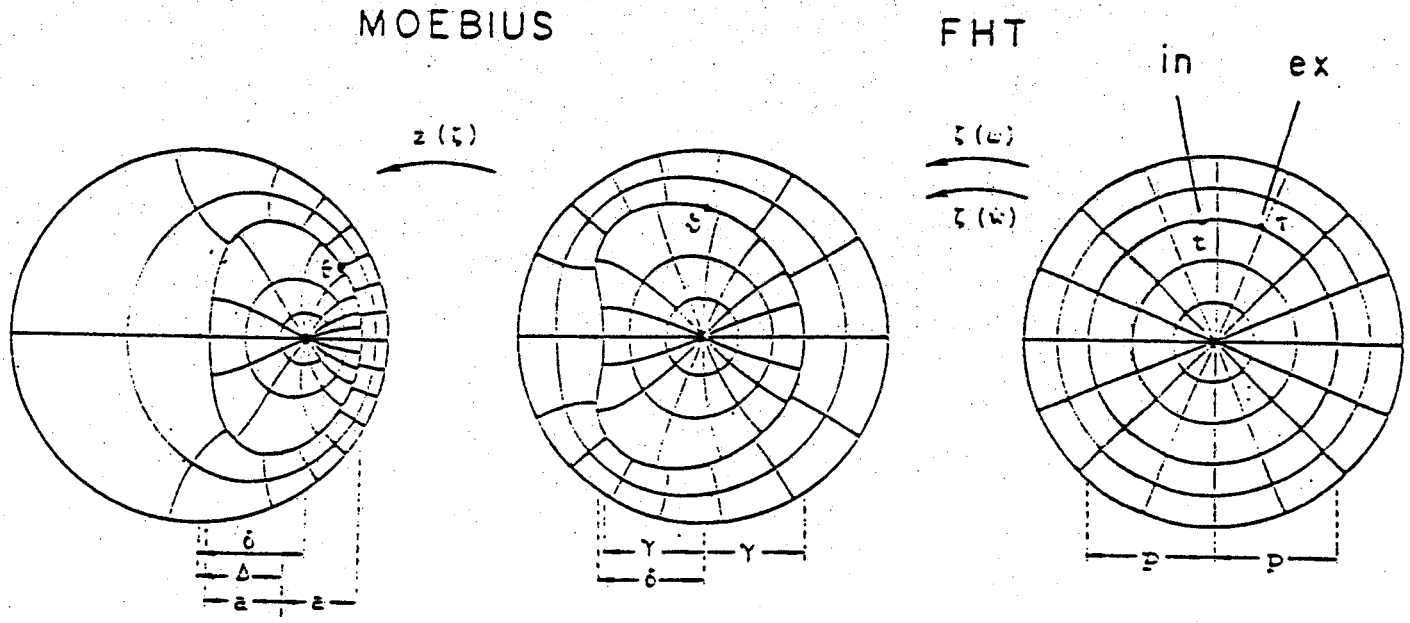

Fig. 17: Complete sequence of conformal mappings for the solution of the stability of free–boundary high–β tokamaks with a skin–current.

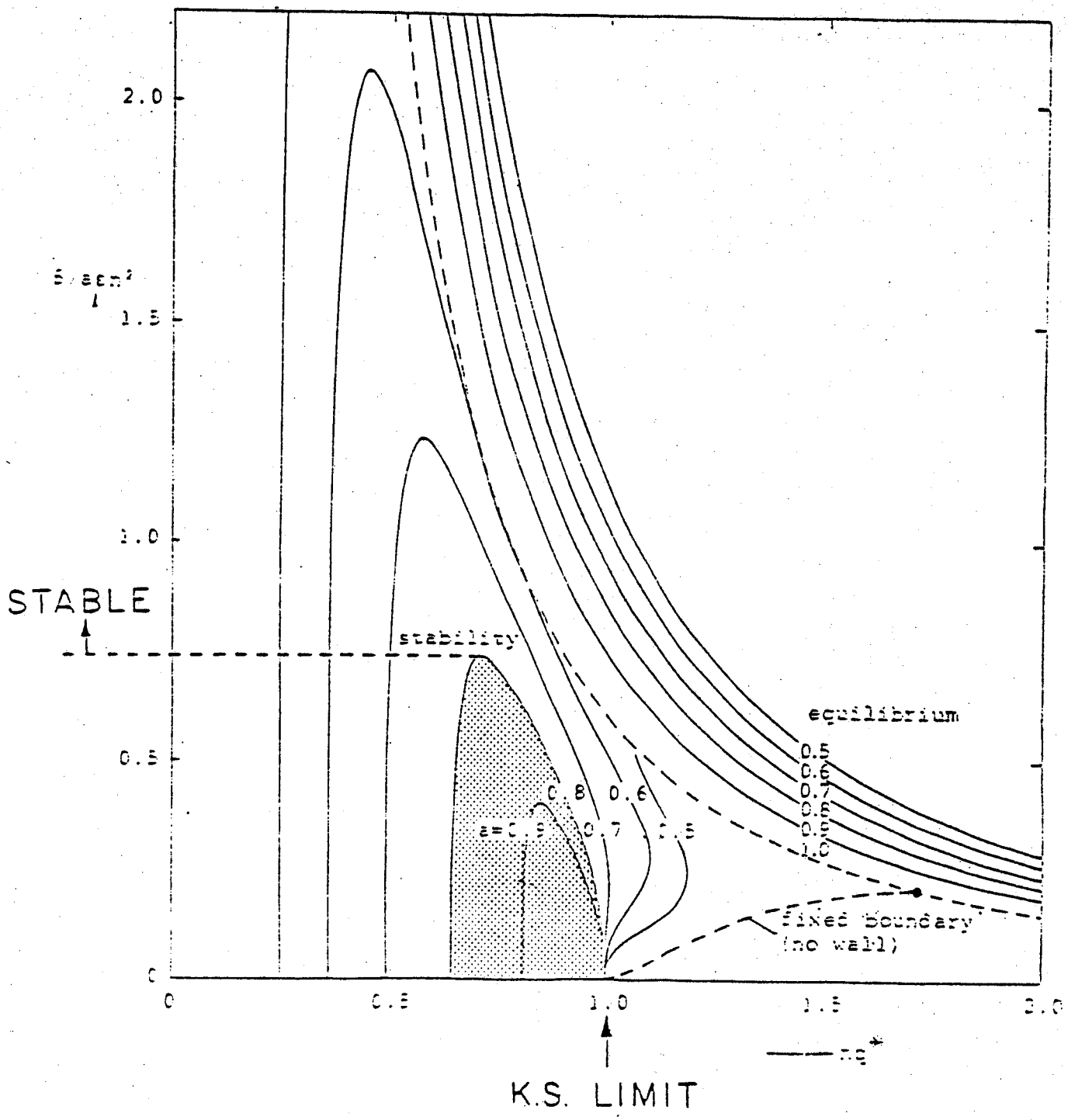

Fig. 18: Stability diagram of free–boundary high–β tokamaks with a skin current.

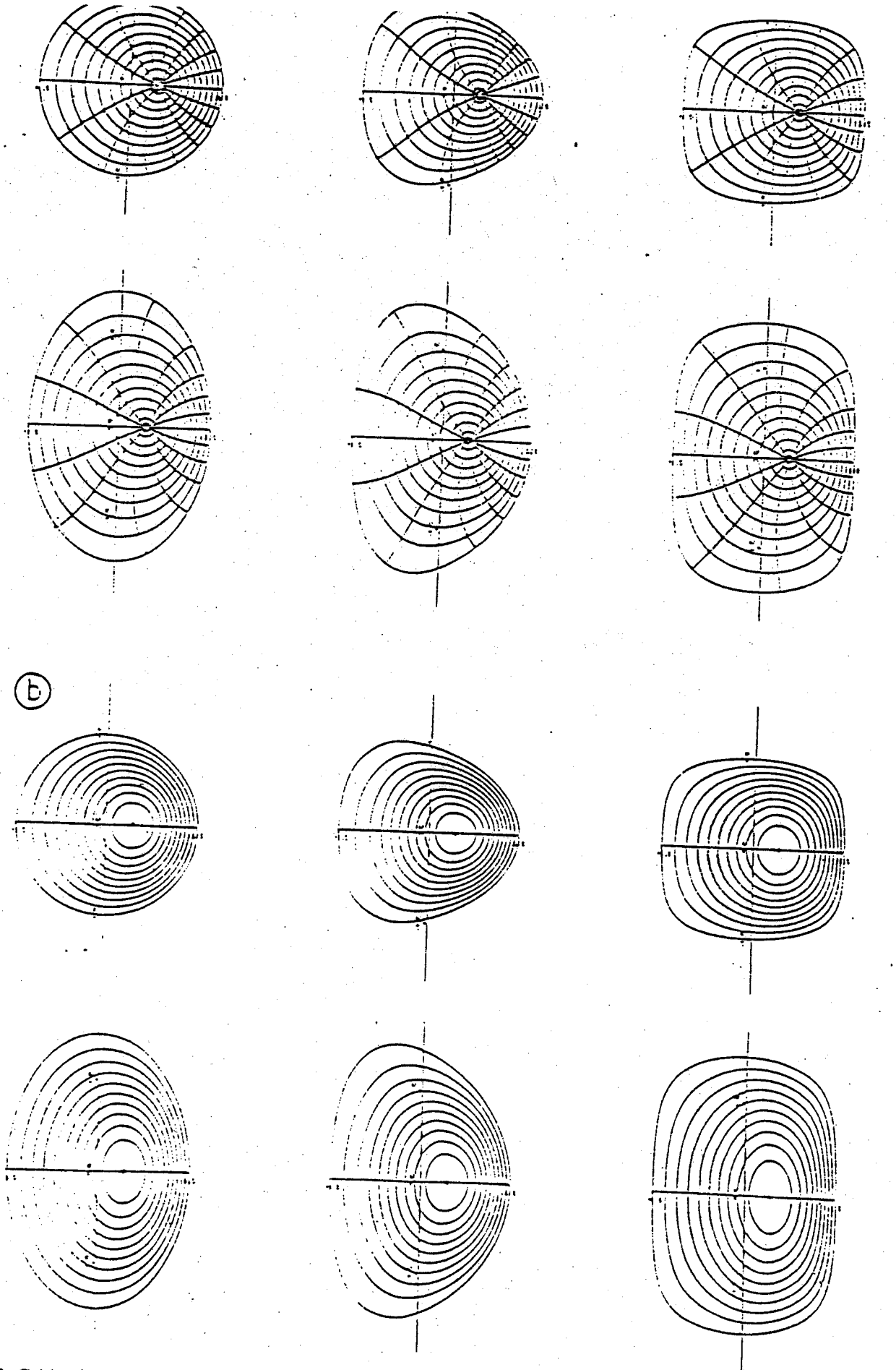

Fig. 19: Grids of the conformal mapping (a) and equilibrium solutions (b) for diffuse high-β tokamaks.

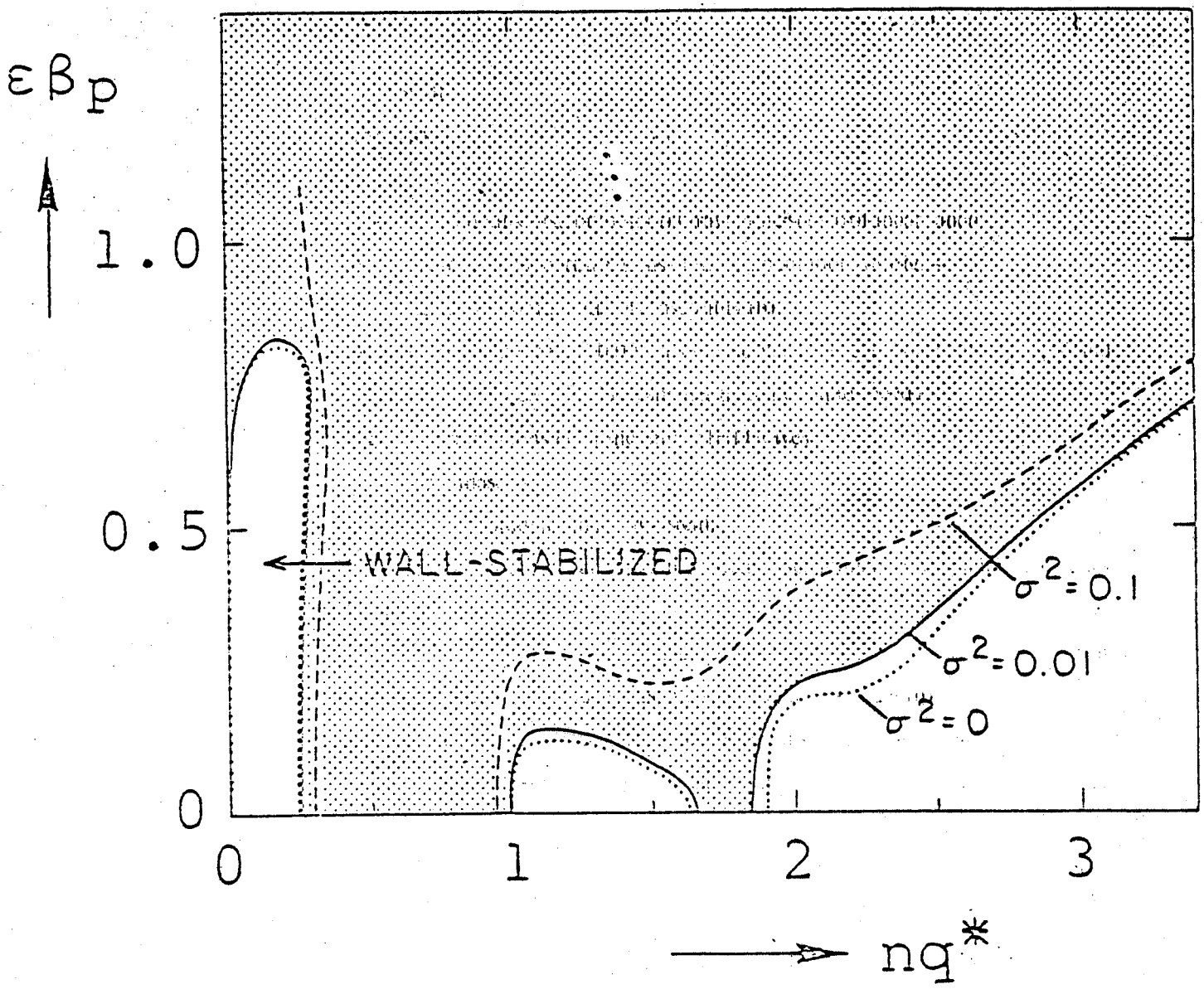

Fig. 20: σ–stability diagram for diffuse high–β tokamak with circular cross–section, $b/a = 2$.

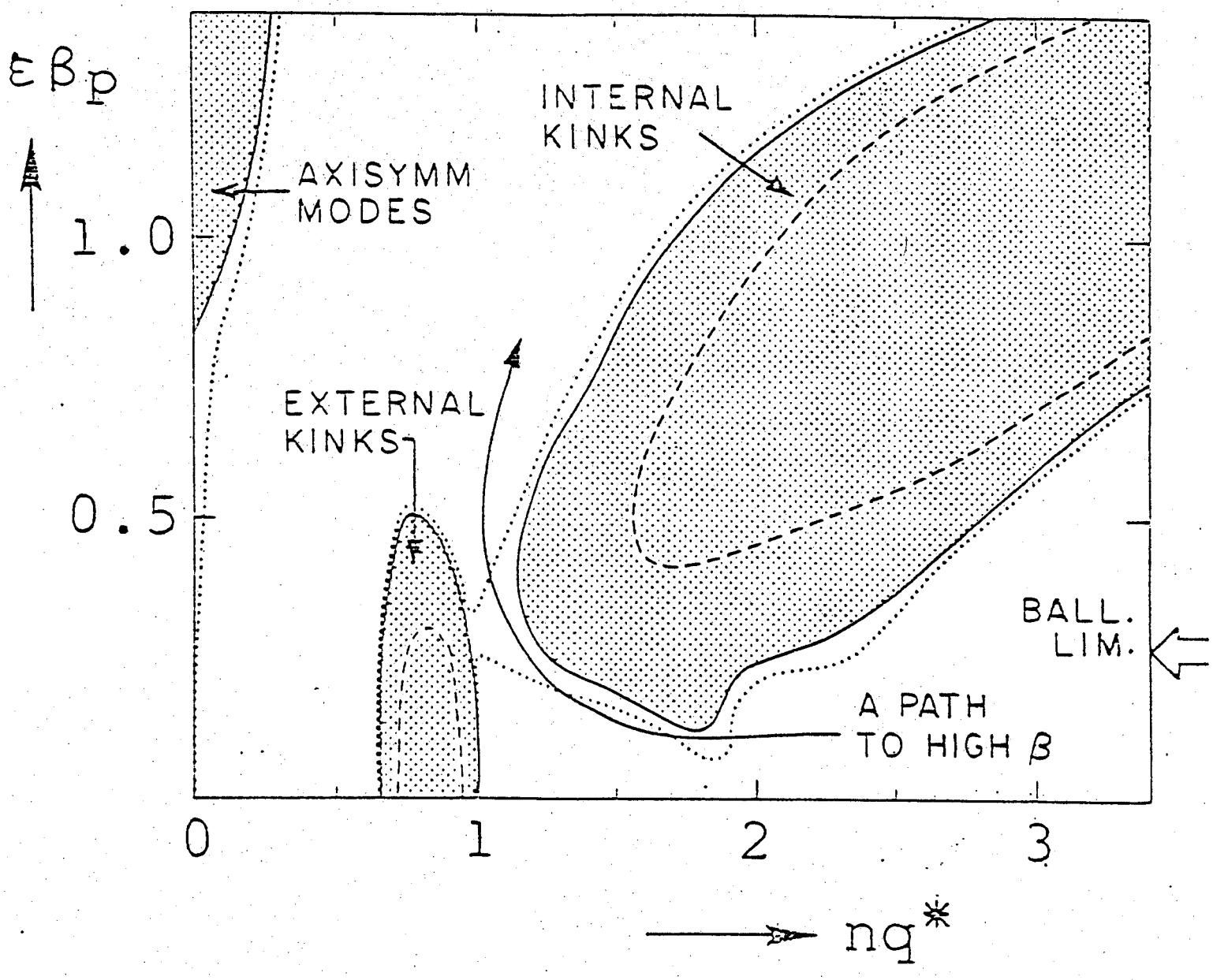

Fig. 21: σ–stability diagram for diffuse high–β tokamak with circular cross–section, $b/a = 1.25$.

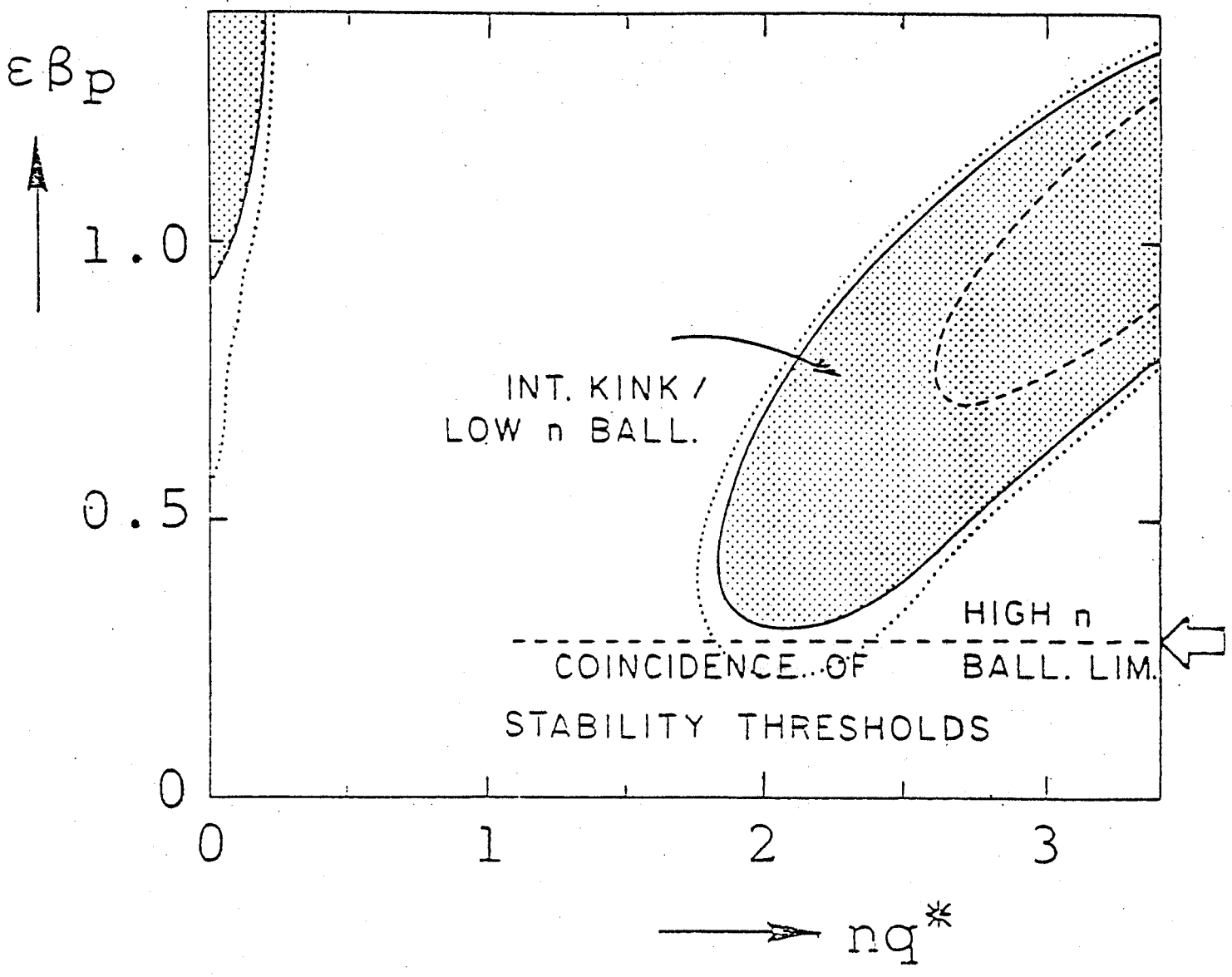

Fig. 22: σ–stability diagram for diffuse high–β tokamak with circular cross–section, $b/a = 1$.

Figure Captions

1 Plasma–vacuum interface system.

2 Toroidal confinement geometry.

3 Field–line topology.

4 Geometries for Rayleigh–Taylor and kink instabilities: (a) Gravitating slab. (b)Linear pinch.

5 Direction of k–vector for the most unstable perturbations of the configurations of Fig. 4.

6 Stability diagrams for the Rayleigh–Taylor (a) and kink instability (b).

7 Phase (a) and group (b) diagrams for the three MHD waves: fast magneto acoustic (F), Alfven (A), and slow magneto acoustic (S). The Alfven speed b is taken smaller than the sound speed c.

8 Displacements ξ and magnetic perturbations Q for the three MHD waves.

9 Projection for inhomogeneous plasmas.

10 Structure of the spectrum of a 1D quantum mechanical system.

11 Structure of the spectrum of a 1D magnetohydrodynamic system. Accumulation of point eigenvalues both from above and below.

12 Typical continuous spectrum of Alfven waves (a) producing a clusterpoint of discrete global Alfven modes and transforming the fast magneto acoustic waves into damped quasi–modes (b).

13 Clusterpoint of slow magneto acoustic and Alfven modes when Suydam's criterion is violated.

14 Conformal mapping of the poloidal cross–section of a toroidal plasma onto a circle with the image of the magnetic axis in the center.

15 Domains for the Fast Hilbert Transformation of analytic functions in simply–connected (a) and doubly–connected (b) regions.

16 (a) Theodorsen's mapping of flow around a wing, (b) Garrick's mapping of flow around a biplane, and (c) superposition of the two to describe the stability of tokamaks.

17 Complete sequence of conformal mappings for the solution of the stability of free–boundary high–β tokamaks with a skin–current.

18 Stability diagram of free–boundary high–β tokamaks with a skin current.

19 Grids of the conformal mapping (a) and equilibrium solutions (b) for diffuse high–β tokamaks obtained from program HBT.

20 σ–stability diagram for diffuse high–β tokamak with circular cross–section, $b/a = 2$.

21 σ–stability diagram for diffuse high–β tokamak with circular cross–section, $b/a = 1.25$.

22 σ–stability diagram for diffuse high–β tokamak with circular cross–section, $b/a = 1$.